^{6}Li/^{7}Li ranges approximately from

$$y_6^{obs}/y_7^{obs} \lesssim 0.5 \quad \text{to} \quad 1.3. \tag{3.6}$$

Note that this constraint lies well above the theoretical ^{6}Li/H curve in Fig. 1.2 for the entire range of η. Since I have only a rough range of upper bounds on ^{6}Li, and no lower bound, I will not use ^{6}Li in my statistical analysis to test the concordance between observation and theory. Instead, I will just check the consistency of my theoretical results with the above constraint.

Chapter 4

Statistical Analysis of Theory and Observation

In this chapter, I describe how I compare my theoretical calculations from Ch. 2 with the observed abundances from Ch. 3 to arrive at meaningful bounds on the properties of the radiatively-decaying X particle. I dwell at some length on this topic, because there has been confusion in the literature as to how to compare theory and observation, and what such comparisons mean. I then discuss my results.

4.1   Analysis

In this section, I seek to answer the question, "How well does my simulation of BBN agree with the observed light-element abundances?" To be more precise, I rephrase the question as, "At what confidence level is my simulation of BBN excluded by the observed light-element abundances?"

From my Monte-Carlo BBN simulation, I obtain the theoretical probability density function (p.d.f.) $p^{th}(\mathbf{a}^{th})$ of the simulated light-element abundances $\mathbf{a}^{th} = (y_2^{th}, Y^{th}, \log_{10} y_7^{th})$. I find that $p^{th}(\mathbf{a}^{th})$ is well-approximated by the product of independent, Gaussian probability distribution functions. [See Eqs. (2.5) and (2.6).] Note that $p^{th}(\mathbf{a}^{th})$ depends upon the parameters $\mathbf{p}$ of my theory, $e.g.$ $\mathbf{p}$

$= (\eta, ...)$. (The ellipses refer to parameters in non-standard BBN, *e.g.*, $m_X Y_X$ and τ_X.) In particular, the means and standard deviations of $p^{th}(\mathbf{a}^{th})$ are functions of **p**.

I also construct the p.d.f. $p^{obs}(\mathbf{a}^{obs})$ for the observed light-element abundances, *viz.*, $\mathbf{a}^{obs} = (y_2^{obs}, Y^{obs}, \log_{10} y_7^{obs})$. Since the observations of the light element abundances are independent, I can factor the joint probability density:

$$p^{obs}(\mathbf{a}^{obs}) = p_2^{obs}(y_2^{obs}) \times p_4^{obs}(Y^{obs}) \times p_7^{obs}(\log_{10} y_7^{obs}). \tag{4.1}$$

I assume Gaussian p.d.f.'s for y_2^{obs}, Y^{obs}, and $\log_{10} y_7^{obs}$. I use the mean abundances and standard deviations given in Equations (3.1)–(3.5). Since I have two discordant values of D/H and two discordant values of ^{4}He, I considered all four cases.

Consider now $\Delta \mathbf{a} = \mathbf{a}^{th} - \mathbf{a}^{obs}$. This quantity has a p.d.f. given by

$$
\begin{aligned}
p^\Delta(\Delta \mathbf{a}) &= \int d\mathbf{a}^{obs} \, p^{obs}(\mathbf{a}^{obs}) \int d\mathbf{a}^{th} \, p^{th}(\mathbf{a}^{th}) \delta(\Delta \mathbf{a} - (\mathbf{a}^{th} - \mathbf{a}^{obs})) \\
&= \int d\mathbf{a} \, p^{th}(\mathbf{a}) p^{obs}(\mathbf{a} - \Delta \mathbf{a}),
\end{aligned}
\tag{4.2}
$$

where I have suppressed the dependence of $p^\Delta(\Delta \mathbf{a})$ and $p^{th}(\mathbf{a}^{th})$ on the theory parameters **p**. Note that when all p_i^{th} and p_i^{obs} are Gaussian, Eq. (4.2) is easily integrated to yield a product of three Gaussian p.d.f.'s:

$$p^\Delta(\Delta \mathbf{a}) = \prod_i \frac{1}{\sqrt{2\pi}\sigma_i} \exp\left[-\frac{(\Delta a_i - \Delta \bar{a}_i)^2}{2\sigma_i^2}\right], \tag{4.3}$$

where $\Delta \bar{a}_i = \bar{a}_i^{th} - \bar{a}_i^{obs}$, $\sigma_i^2 = (\sigma_i^{th})^2 + (\sigma_i^{obs})^2$ and i runs over $(y_2, Y, log_{10}y_7)$.

My question can now be rephrased as, "At what confidence level (C.L.) is

$\Delta a = 0$ excluded?" The answer,

$$\text{C.L.}(\mathbf{p}) = \int_{\{\Delta a : p^\Delta(\Delta a; \mathbf{p}) > p^\Delta(0; \mathbf{p})\}} d(\Delta a)\, p^\Delta(\Delta a; \mathbf{p}), \qquad (4.4)$$

is used in this dissertation to constrain various scenarios of BBN. Since I have assumed Gaussian p.d.f.'s, I can easily evaluate this integral. The result is conveniently expressed in terms of a χ^2 function of the abundances:

$$\text{C.L.} = \int_0^{\chi^2} \frac{1}{2^{3/2}\Gamma(\frac{3}{2})} y^{\frac{1}{2}} e^{-\frac{y}{2}} dy \qquad (4.5)$$

$$= -\sqrt{\frac{2\chi^2}{\pi}} \exp\left(-\frac{\chi^2}{2}\right) + \text{erf}\left(\sqrt{\frac{\chi^2}{2}}\right), \qquad (4.6)$$

where

$$\chi^2 = \sum_i \frac{(a_i^{th} - a_i^{obs})^2}{(\sigma_i^{th})^2 + (\sigma_i^{obs})^2}, \qquad (4.7)$$

for $a_i = (y_2, Y, \log_{10} y_7)$, and $(\sigma_i^{obs})^2 = (\sigma_i^{syst})^2 + (\sigma_i^{stat})^2$.

The confidence level is calculated for three degrees of freedom Δa_i. It denotes the certainty that a given point $\mathbf{p}$ in the parameter space of the theory is excluded by the observed abundances. In order to compare my theory with a late-decaying particle (three parameters $\mathbf{p}$: $\tau_X, m_X Y_X$, and η) to a theory with a different number of parameters (e.g., only one in SBBN), one would want to use a χ^2 variable in these parameters. This transformation would be possible if the abundances a_i were linear in the theory parameters $\mathbf{p}$. In that case, I could integrate out a theory parameter such as η and set a C.L. exclusion limit (with a reduced number of degrees of freedom) on the remaining parameters. However, the a_i turn out to be highly non-linear functions of $\mathbf{p}$, so integrating out a theory parameter turns

51

out to have little meaning. Instead, I shall project out various theory parameters (as explained in Section 4.2.1) to present my results as graphs.

4.2 Results

As I mentioned in Section 3.1, I have two ^{4}He values that have been inferred from various observed data to be the primordial components. I also have two primordial D/H values, which are deduced from the spectra of quasar absorption systems (QAS). In this section, I compare the theoretical calculations with these observed abundances and show how I can constrain the model parameters in each of the four cases.

4.2.1 Low ^{4}He ($Y^{obs} = 0.234 \pm (0.002)_{stat} \pm (0.005)_{syst}$)

Recalling that the low observed ^{4}He value [Eq. (3.3)] is consistent with the theoretical calculation at low η in the case of SBBN, I expect that I can obtain rigid constraints on the model parameters for the high observed D/H value [Eq. (3.2)]. On the other hand, for the low observed D/H value [Eq. (3.1)], I search the parameter space for regions of better fit than I can obtain with SBBN.

Low QAS D/H ($y_2^{obs} = (3.39 \pm 0.25) \times 10^{-5}$)

In Fig. 4.1, I show the contours of the confidence level computed using three elements (D, ^{4}He, and ^{7}Li) for some representative η values ($2 \times 10^{-10}, 4 \times 10^{-10}, 5 \times 10^{-10}, 6 \times 10^{-10}$). The region of parameter space that is allowed at the 68%

C.L. extends down to low η (see Fig. 4.1a). Near $\eta = 2 \times 10^{-10}$, deuterium is destroyed by an order of magnitude (without net destruction of ^{4}He), so that the remaining deuterium agrees with the calculated low ^{4}He. I also plotted the regions excluded by the observational upper bounds on ^{6}Li/^{7}Li. The shaded regions are $y_6/y_7 \gtrsim 0.5$, and the darker shaded regions are $y_6/y_7 \gtrsim 1.3$. Even if I adopt the stronger bound $y_6/y_7 \lesssim 0.5$, my constraints from the other elements are consistent with the observed ^{6}Li value.

In Fig. 4.2, I show the contours of the confidence levels for various lifetimes, $\tau_X = 10^4, 10^5, 10^6$ sec. As the lifetime decreases, the background temperature at the time of decay increases, so the threshold energy of double-photon pair creation decreases. Then, for a fixed $m_X Y_X$, the number of photons contributing to D destruction decreases. Thus, for shorter lifetimes, I need larger $m_X Y_X$ in order to destroy sufficient amounts of D. The observed abundances prefer non-vanishing $m_X Y_X$.

In Fig. 4.3, I show the edges of the projections of the C.L. regions into the $m_X Y_X$ vs. τ_X plane. By projection, I mean taking the lowest C.L. value for a fixed point $(\tau_X, m_X Y_X)$ as η varies.

The lower $m_X Y_X$ region, i.e., $m_X Y_X \sim 10^{-14}$ GeV, corresponds to SBBN, since there are not enough high-energy photons to affect the light-element abundances. It is notable that these regions are outside of the 68% C.L. This fact may suggest the existence of a long-lived massive particle X, and may be regarded as a hint of physics beyond the standard model or standard big-bang cosmology.

53

For example, in Fig. 4.4 I show the predicted abundances of ^{4}He, D/H, ^{7}Li/H, and ^{6}Li/H, adopting the model parameters $\tau_X = 10^6$ sec and $m_X Y_X = 5 \times 10^{-10}$ GeV. This point lies within the 68% C.L., as seen in Fig. 4.3. The predicted abundances of ^{4}He and ^{7}Li are nearly the same as in SBBN. Only D is significantly destroyed; its abundance decreases by about 80%. At low $\eta \sim (1.7 - 2.3) \times 10^{-10}$ in this model, the predicted abundances of these three elements agree with the observed values. It is interesting that the produced ^{6}Li abundance can be two orders of magnitude larger than the SBBN prediction in this parameter region. The origin of the observed ^{6}Li abundance ^{6}Li/H $\sim O(10^{-12})$ is usually explained by cosmic ray spallation; however, my model demonstrates the possibility that ^{6}Li may have been produced by the photodissociation of ^{7}Li at an early epoch. My ^{6}Li prediction is consistent with the upper bound Eq. (3.6).

Although $m_X Y_X \gtrsim 10^{-10}$ GeV is preferred, it is worth noting that SBBN lies within the 95% C.L. agreement between theory and observation. In Fig. 4.3, the 95% bound for $\tau_X \lesssim 10^6$ sec comes from the constraint that not much more than 90% of the deuterium should be destroyed; for $\tau_X \gtrsim 10^6$ sec the constraint is that deuterium should not be produced from ^{4}He photofission. In Table 4.1, I show the representative values of $m_X Y_X$ that correspond to the 68% and 95% confidence levels respectively, for $\tau_X = 10^4 - 10^9$ sec.

High QAS D/H ($y_2^{obs} = (1.9 \pm 0.5) \times 10^{-4}$)

In the case of low ^{4}He and high D/H, SBBN (*i.e.*, low $m_X Y_X$) works quite well

$\tau_X =$	10^4 sec	10^5 sec	10^6 sec	10^7 sec	10^8 sec	10^9 sec
95% C.L.	9×10^{-6}	9×10^{-9}	1×10^{-9}	7×10^{-11}	2×10^{-12}	7×10^{-13}
68% C.L.	$\{{}^9_1\}\times10^{-6}$	$\{{}^7_1\}\times10^{-9}$	$\{{}^9_2\}\times10^{-10}$			

Table 4.1: Upper or (lower – upper) bound on $m_X Y_X$ in units of GeV for the case of low ^{4}He and low D/H. Note that the C.L. is for three degrees of freedom, and η is varied to give the extreme values for $m_X Y_X$.

for $\eta \sim 2 \times 10^{-10}$. Thus, I expect that I can strongly bound the parameter space of the X-decay model. In Fig. 4.5, I show the 68% and 95% C.L. contours for some representative values of η. At low η, I obtain an upper bound on ^{4}He, primarily from the constraint on D/H (Fig. 4.5a).

There are also allowed (at better than the 68% C.L.) regions of parameter space at higher values of eta (see Figs. 4.5b–4.5d). These allowed regions lie at $\tau_X \gtrsim 10^6$ sec where a small amount of ^{4}He is broken down into D. However, these allowed regions are small, because the parameters must be finely tuned to target the D/H abundance to $\sim O(10^{-4})$.

In Fig. 4.6, I show the contour plots for some representative τ_X in the same manner as in Fig. 4.2.

In Fig. 4.7, I plot the contours projected along the η axis in a fashion similar to Fig. 4.3. Comparing the constraints on τ_X and $m_X Y_X$ with the case of low D/H (Fig. 4.3), I find that the 95% boundary is moved to higher $m_X Y_X$, for $\tau_X \gtrsim 10^6$ sec. This is because D (produced by ^{4}He destruction) is permitted to be an order of magnitude more abundant than in the case of the low D/H observation. I show the 68% and 95% C.L. upper bounds on $m_X Y_X$ in Table 4.2 for various

$\tau_X =$	10^4 sec	10^5 sec	10^6 sec	10^7 sec	10^8 sec	10^9 sec
95% C.L.	5×10^{-6}	5×10^{-9}	6×10^{-10}	5×10^{-10}	7×10^{-11}	4×10^{-11}
68% C.L.	3×10^{-6}	3×10^{-9}	3×10^{-10}	4×10^{-10}	5×10^{-11}	3×10^{-11}

Table 4.2: Same as Table 4.1, except for low ^{4}He and high D/H.

lifetimes τ_X.

4.2.2 High ^{4}He ($Y^{obs} = 0.244 \pm (0.002)_{stat} \pm (0.005)_{syst}$)

The high observed ^{4}He abundance [Eq. (3.4)] is consistent with the SBBN theoretical calculations for both the low and high observed D/H abundances [Eqs. (3.1) and (3.2)]. Therefore, I expect to be able to constrain the model parameters in both cases.

Low QAS D/H ($y_2^{obs} = (3.39 \pm 0.25) \times 10^{-5}$)

For four representative η values $(2 \times 10^{-10}, 4 \times 10^{-10}, 5 \times 10^{-10}, 6 \times 10^{-10})$, I plot the contours of the confidence level in Fig. 4.8. In Fig. 1.2, one can see that the SBBN calculations agree with the observed abundances for mid-range values of the baryon-to-photon ratio ($\eta \sim 5 \times 10^{-10}$). Thus, the upper bound for $m_X Y_X$ is plotted in Fig. 4.8c. Even at a low η (where the SBBN calculation disagrees with the low observed D/H value), the theoretical calculations can match observed data in the region 10^4 sec $\lesssim \tau_X \lesssim 10^6$ sec and $m_X Y_X \gtrsim 10^{-10}$ because of the significant destruction of D. In Fig. 4.9, I show the C.L. plots for three typical lifetimes, $\tau_X = 10^4, 10^5, 10^6$ sec. Finally, I show the C.L. contours projected along the η

56

$\tau_X =$	10^4 sec	10^5 sec	10^6 sec	10^7 sec	10^8 sec	10^9 sec
95% C.L.	7×10^{-6}	7×10^{-9}	8×10^{-10}	1×10^{-10}	8×10^{-12}	3×10^{-12}
68% C.L.	5×10^{-6}	5×10^{-9}	6×10^{-10}	8×10^{-11}	4×10^{-12}	2×10^{-12}

Table 4.3: Same as Table 4.1, except for high ^{4}He and low D/H.

axis into the $m_X Y_X$ vs. τ_X plane (Fig. 4.10). Table 4.3 gives the upper bounds on $m_X Y_X$ (in GeV) that correspond to the 68% and 95% C.L., for some typical values of the lifetime.

High QAS D/H ($y_2^{obs} = (1.9 \pm 0.5) \times 10^{-4}$)

As in the low D/H case, I now plot C.L. contours for high D/H for four typical values of η in Fig. 4.11. Since the high ^{4}He and high D/H observed values are consistent with SBBN calculations for low η, I expect to obtain bounds on τ_X and $m_X Y_X$ (e.g., , Fig. 4.11a). In Figs. 4.11b – 4.11d, I see that I also have allowed regions for $\tau_X \gtrsim 10^6$ sec. The reason is same as in the case of low ^{4}He and high D/H; the final D/H abundances are well-balanced between production and destruction.

In Fig. 4.12, I plot the confidence level for $\tau_X = 10^4, 10^5$, and 10^6 sec. The range of preferred η at the 68% C.L. is relatively narrow, compared to the case of high D/H and low ^{4}He. This is because the case of high D/H and high ^{4}He is only consistent in SBBN for low values of η, and in the lifetime range $\tau_X \sim 10^4 - 10^6$, the ^{4}He abundance is not affected by the radiative decay of X.

Next, I show the 68% and 95% C.L. contours projected along the η axis

$\tau_X =$	10^4 sec	10^5 sec	10^6 sec	10^7 sec	10^8 sec	10^9 sec
95% C.L.	2×10^{-6}	3×10^{-9}	3×10^{-10}	4×10^{-10}	5×10^{-11}	3×10^{-11}
68% C.L.	5×10^{-7}	6×10^{-10}	7×10^{-11}	2×10^{-11}	1×10^{-11}	2×10^{-11}

Table 4.4: Same as Table 4.1, except for high ^{4}He and high D/H.

(Fig. 4.13). There is a large region between the 68% C.L. and the 95% (for a fixed τ_X) for two reasons. First, the uncertainty in the high observed D/H value is large. Second, the η predicted from the high observed ^{4}He value has a wide spread. The overall shape of the 95% C.L. line is very similar to the case of low ^{4}He and high D/H. This is because the constraint for $\tau_X \gtrsim 10^6$ sec is particularly sensitive only to the observed D/H value.

Just as in the case of low ^{4}He, the 95% C.L. contour for the high D/H value extends to higher $m_X Y_X$ than for the low D/H value, because the new D component produced by ^{4}He destruction is allowed to be one order of magnitude larger than in the case of low D/H. In Table 4.4, I list the upper bounds on $m_X Y_X$ at the 68% and 95% confidence levels, for various values of τ_X.

4.3 Additional Constraints

I now mention additional constraints on my model. First, the the cosmic microwave background radiation (CMBR) was observed by COBE [2] to very closely follow a blackbody spectrum. This gives us a severe constraint on particles with lifetime longer than $\sim 10^6$ sec [77], which is when the double Compton

process ($\gamma + e^- \rightleftharpoons \gamma + \gamma + e^-$) freezes out [78].[1] After this time, photon number is conserved, so photon injection from a radiatively decaying particle would cause the spectrum of the CMBR to assume a Bose-Einstein distribution with a finite chemical potential μ. COBE [2] observations give us the constraint $|\mu| \lesssim 9.0 \times 10^{-5}$. For small μ, the ratio of the injected to total photon energy density is given by $\delta\rho_\gamma / \rho_\gamma \sim 0.71\mu$. Thus, I have the constraint

$$m_X Y_X \lesssim 6 \times 10^{-10} \text{ GeV} \left(\frac{\tau_X}{10^6 \text{ sec}}\right)^{-\frac{1}{2}} \quad \text{for } 10^6 \text{ sec} \lesssim \tau_X \lesssim 4 \times 10^{10} \text{ sec}. \quad (4.8)$$

Note that for lifetimes τ_X longer than 10^6 sec, the CMBR constraint is comparable to or slightly stricter than the bounds from BBN that I have discussed above.

In this thesis, I have considered only radiative decays, $i.e.$, decays to photons and invisible particles. If X decays to charged leptons, the effect is similar to decay to photons, because the charged leptons also generate soft photons in electromagnetic cascade showers. On the other hand, if X decays only to neutrinos, the constraints becomes much weaker. If, for example, X is the gravitino in the minimal supersymmetric standard model, then it decays into a neutrino and its superpartner, the sneutrino. The emitted neutrinos scatter off the background neutrinos, producing electron-positron pairs that trigger electromagnetic cascades. But because the interaction between the emitted neutrino and the background neutrinos is weak, the destruction of the light elements does not occur very effi-

---

[1]This constraint applies only to particles with lifetime shorter than $\sim 4 \times 10^{10}$ sec, which corresponds to the decoupling time of Compton/inverse Compton scattering. After this time, injected photons do not thermalize with the CMBR.

ciently [79]. On the other hand, if X decays to hadrons, I expect that my bounds would tighten, because hadronic showers could be a significant source of D, ^{3}He, ^{6}Li, ^{7}Li, and ^{7}Be [10]. In fact, even though I have assumed that X decays only to photons, these photons may convert to hadrons in loop diagrams. Thus, the branching ratio to hadrons is at least of order 1%, if kinematically allowed [11]. Therefore, my photodissociation bounds in this dissertation are conservative.

Figure 4.1: C.L. in the $m_X Y_X$ vs. τ_X plane, for low value of ^{4}He and low value of D/H. I take (a) $\eta = 2 \times 10^{-10}$, (b) $\eta = 4 \times 10^{-10}$, (c) $\eta = 5 \times 10^{-10}$, and (d) $\eta = 6 \times 10^{-10}$. The shaded regions are $y_6/y_7 \gtrsim 0.5$, and the darker shaded regions are $y_6/y_7 \gtrsim 1.3$.
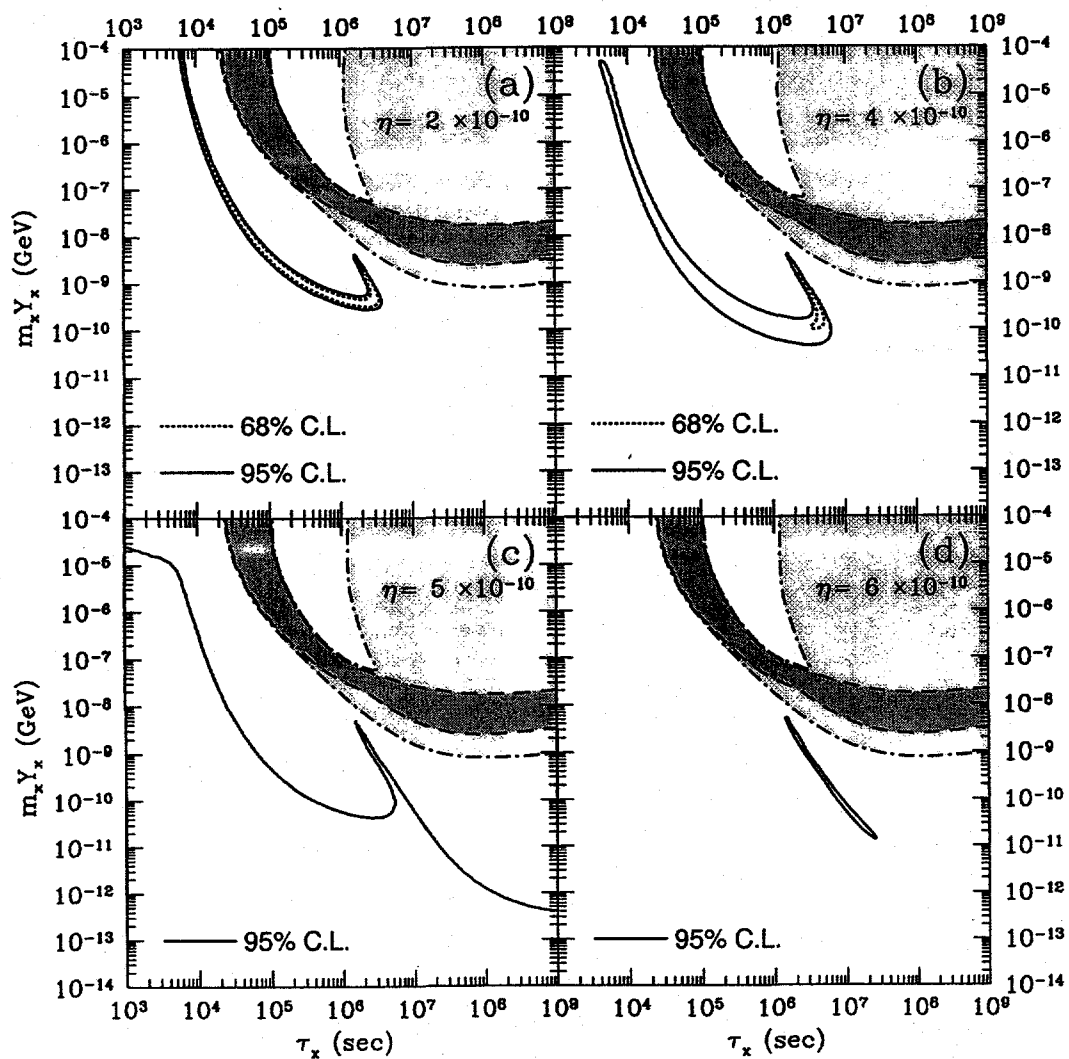
Figure 4.2: C.L. in the $m_X Y_X$ vs. η plane for various values of τ_X, for low value of ^{4}He and low value of D/H.
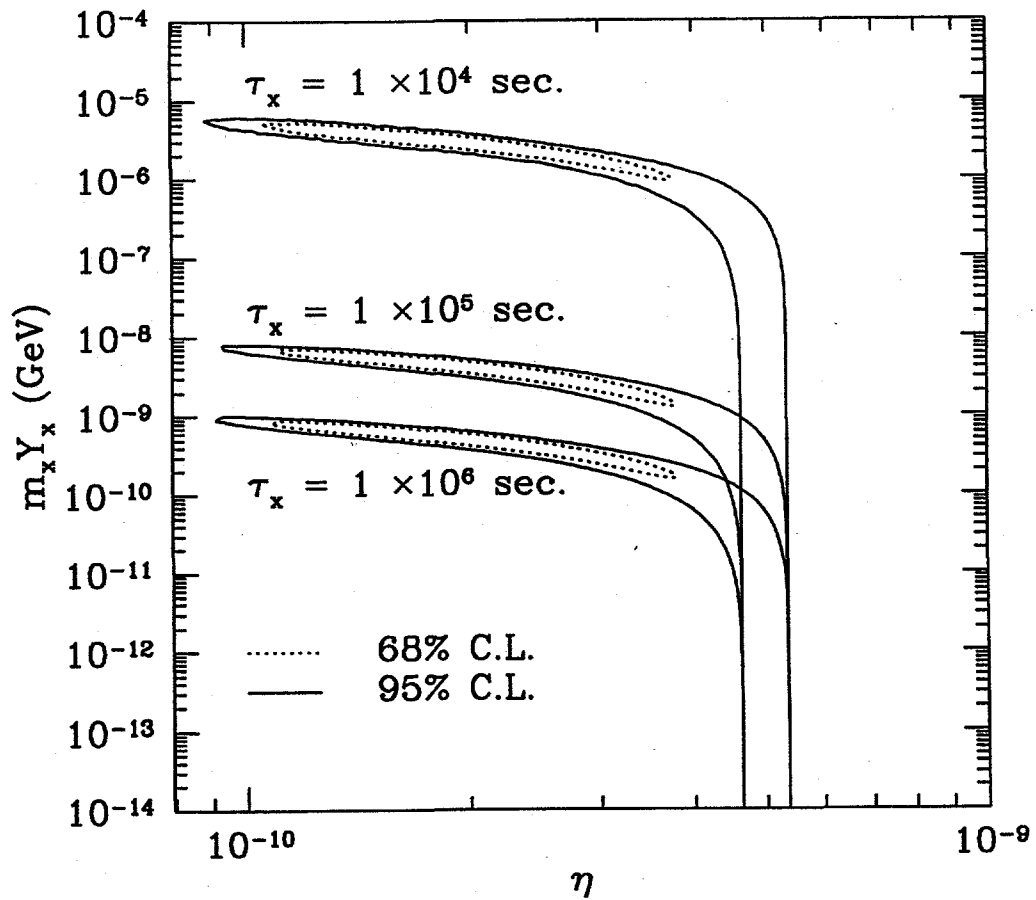
Figure 4.3: Contours of C.L. projected along the η axis, for low value of ^{4}He and low value of D/H.
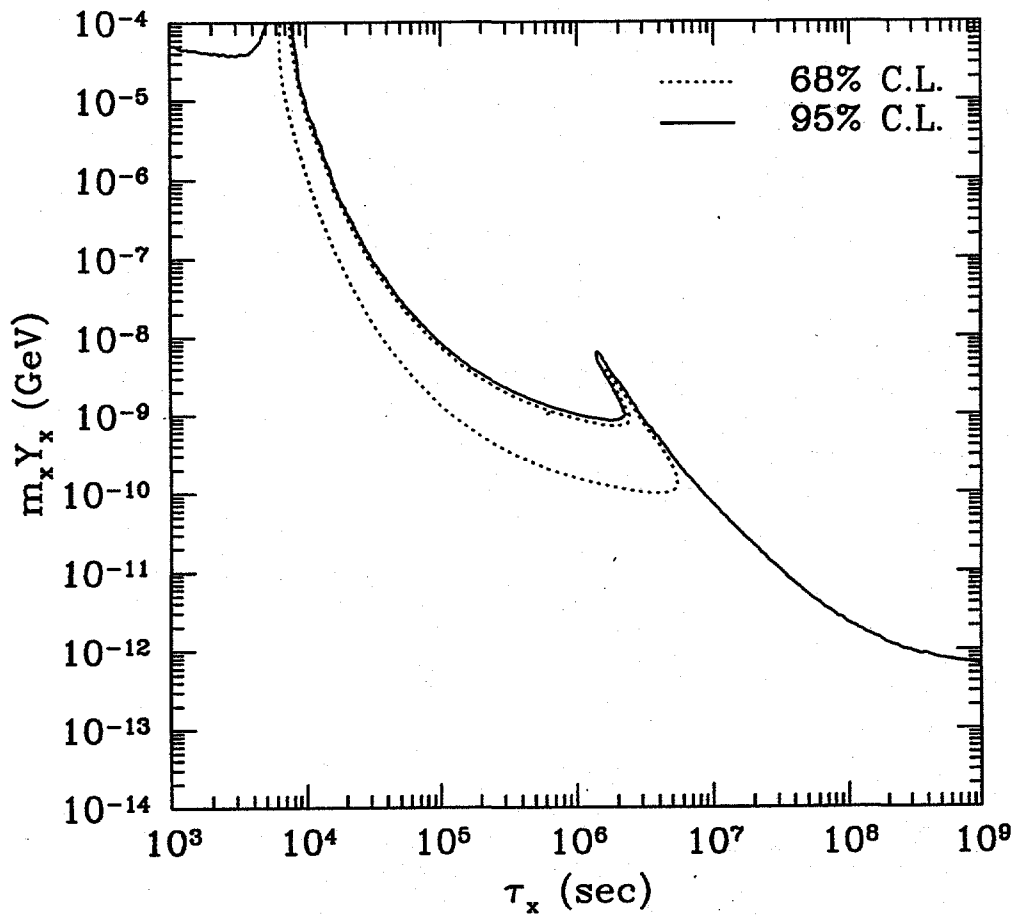
Figure 4.4: Predicted abundances of ^{4}He, D/H, ^{7}Li/H and ^{6}Li/H at $\tau_X = 10^6$ sec and $m_X Y_X = 5 \times 10^{-10}$ GeV. I have indicated the regions that are favored by the low ^{4}He and low D/H observations. The dotted line denotes the 95% C.L., and the shaded region denotes the 68% C.L. The predicted ^{6}Li abundance is two orders of magnitude larger than it is in SBBN.
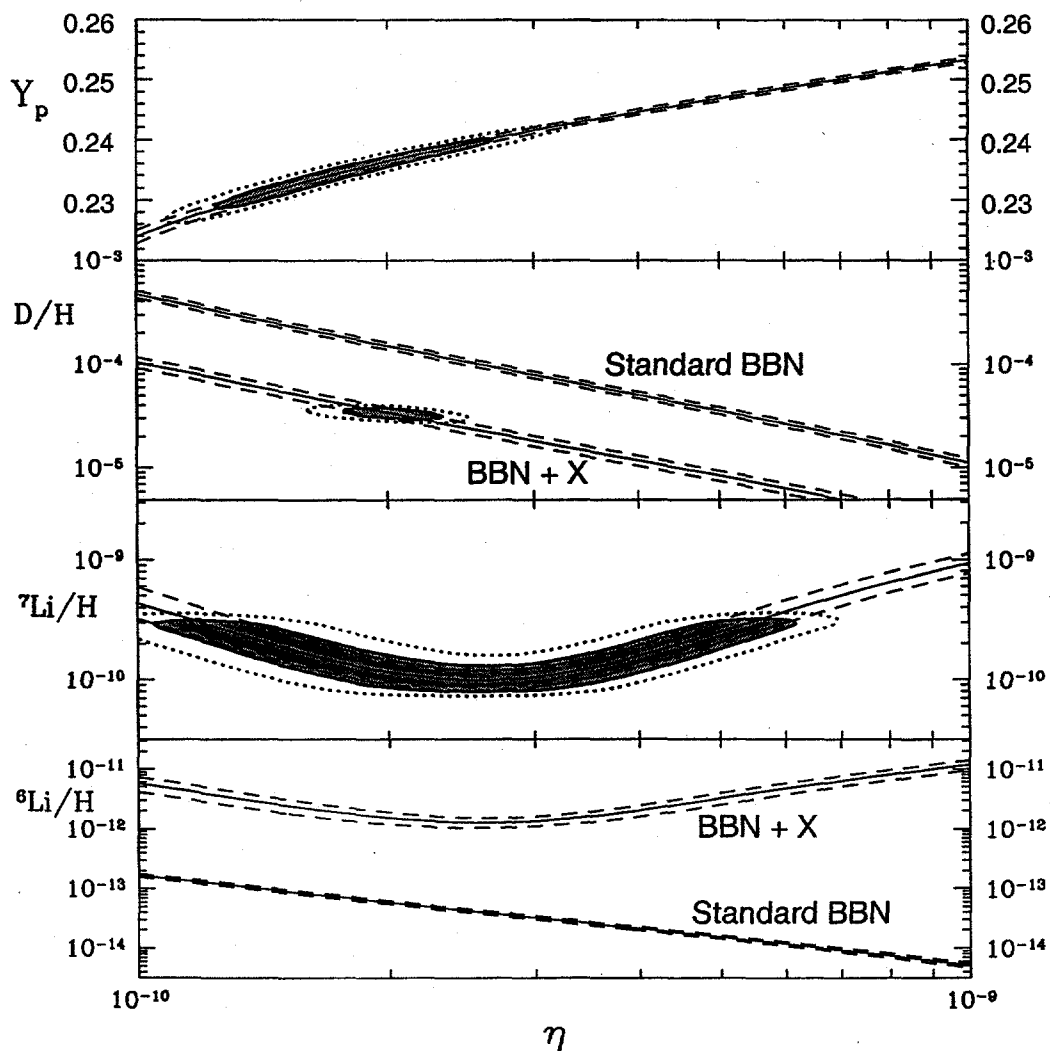
Figure 4.5: Same as Fig. 4.1, except for low value of ^{4}He and high value of D/H.
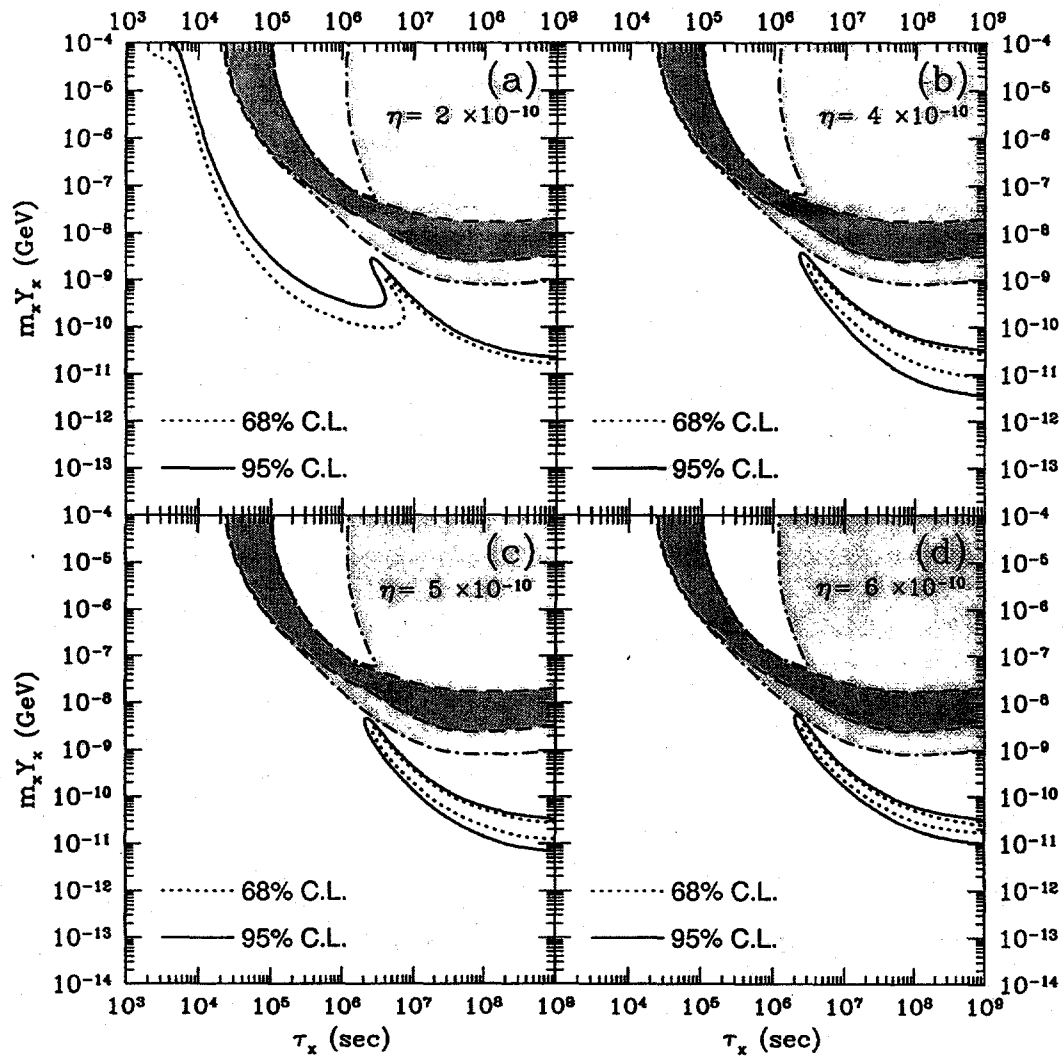
Figure 4.6: Same as Fig. 4.2, except for low value of ^{4}He and high value of D/H.
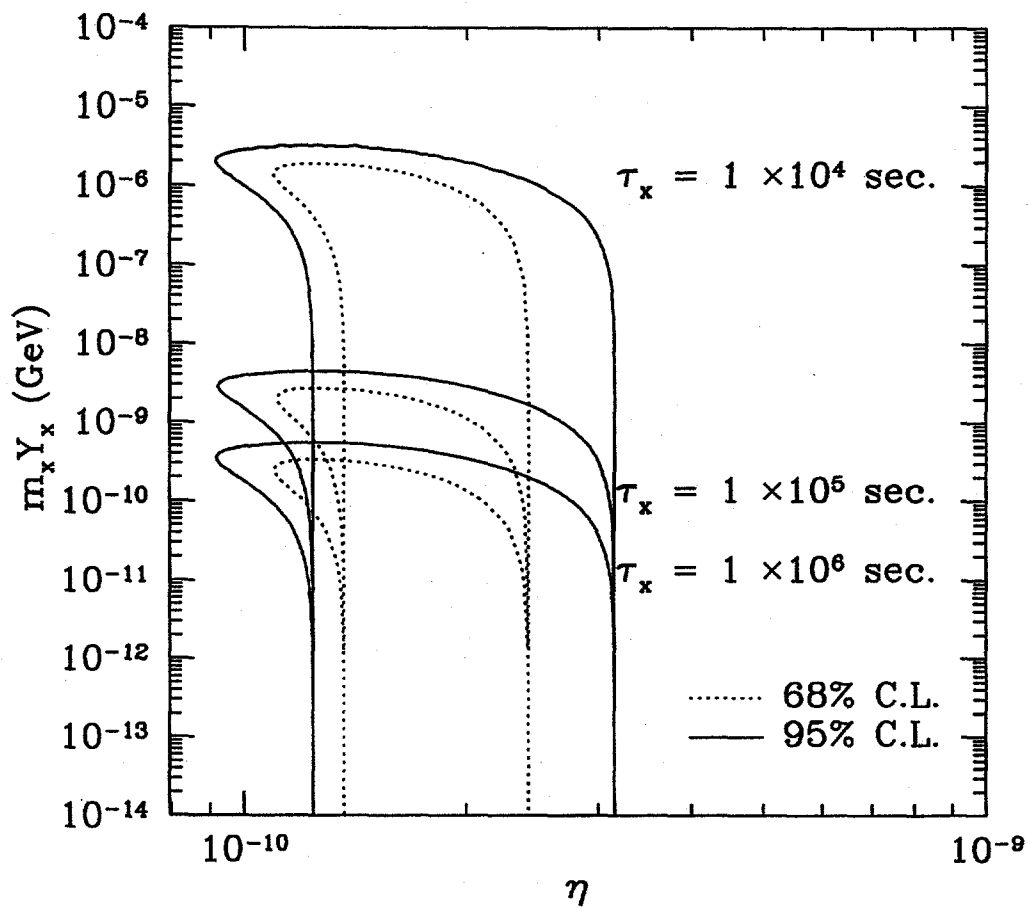
Figure 4.7: Same as Fig. 4.3, except for low value of ^{4}He and high value D/H.
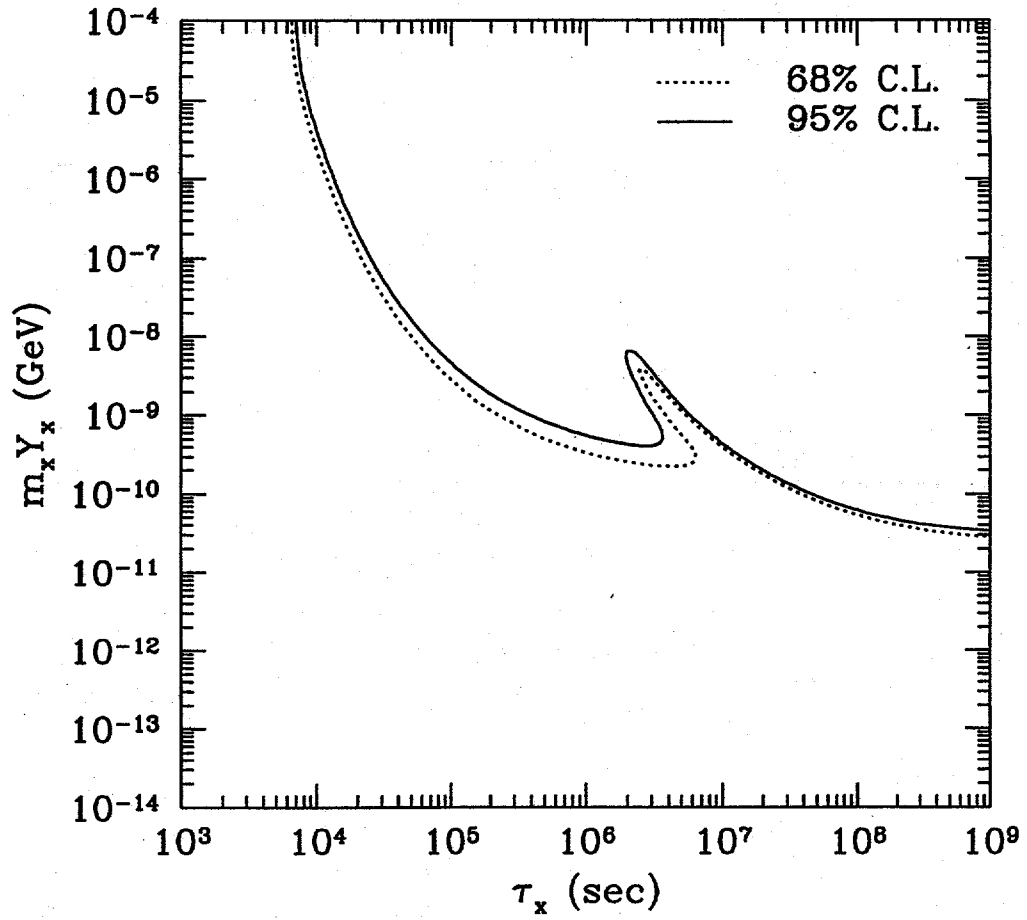
Figure 4.8: Same as Fig. 4.1, except for high value of ^{4}He and low value of D/H.
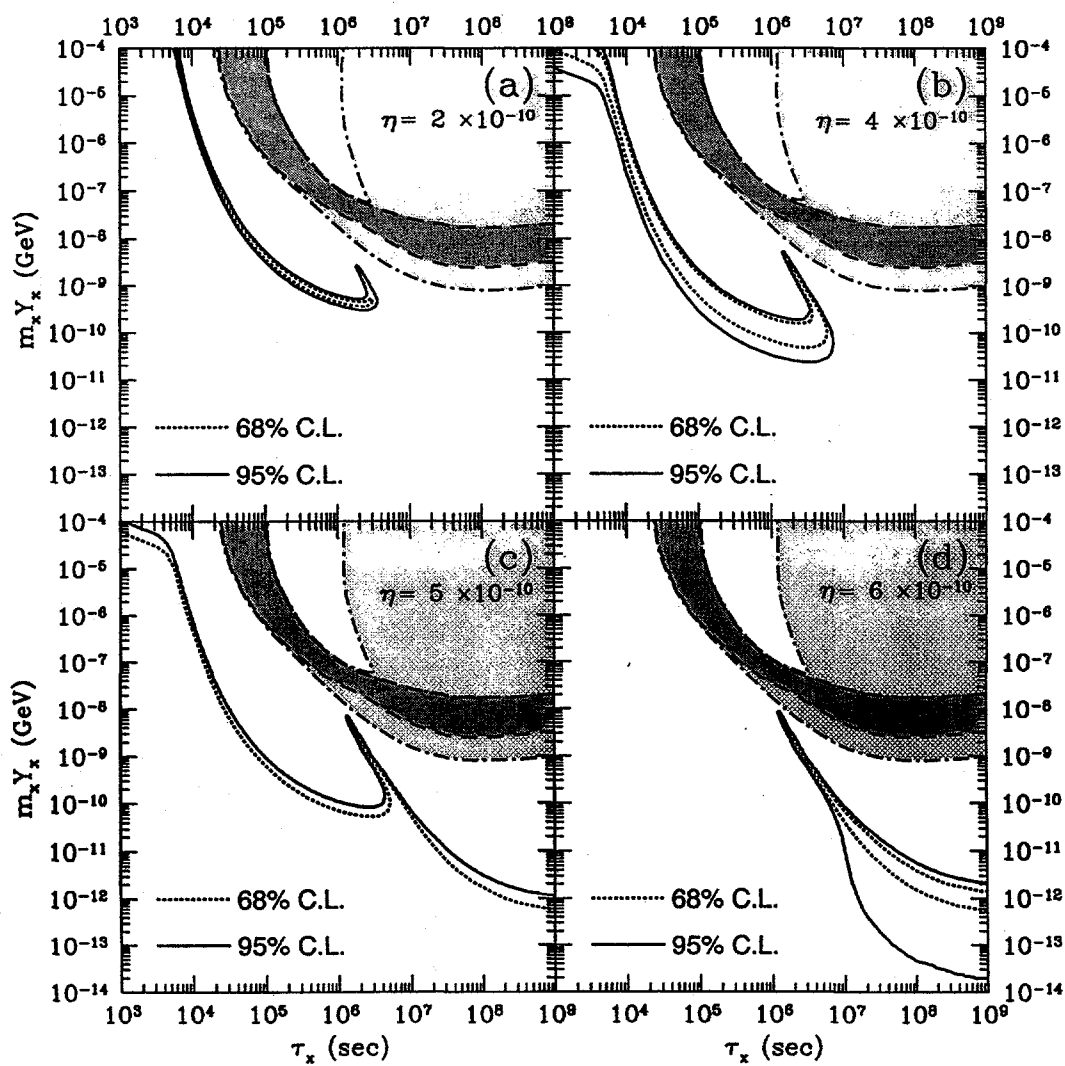
Figure 4.9: Same as Fig. 4.2, except for high value of ^{4}He and low value of D/H.
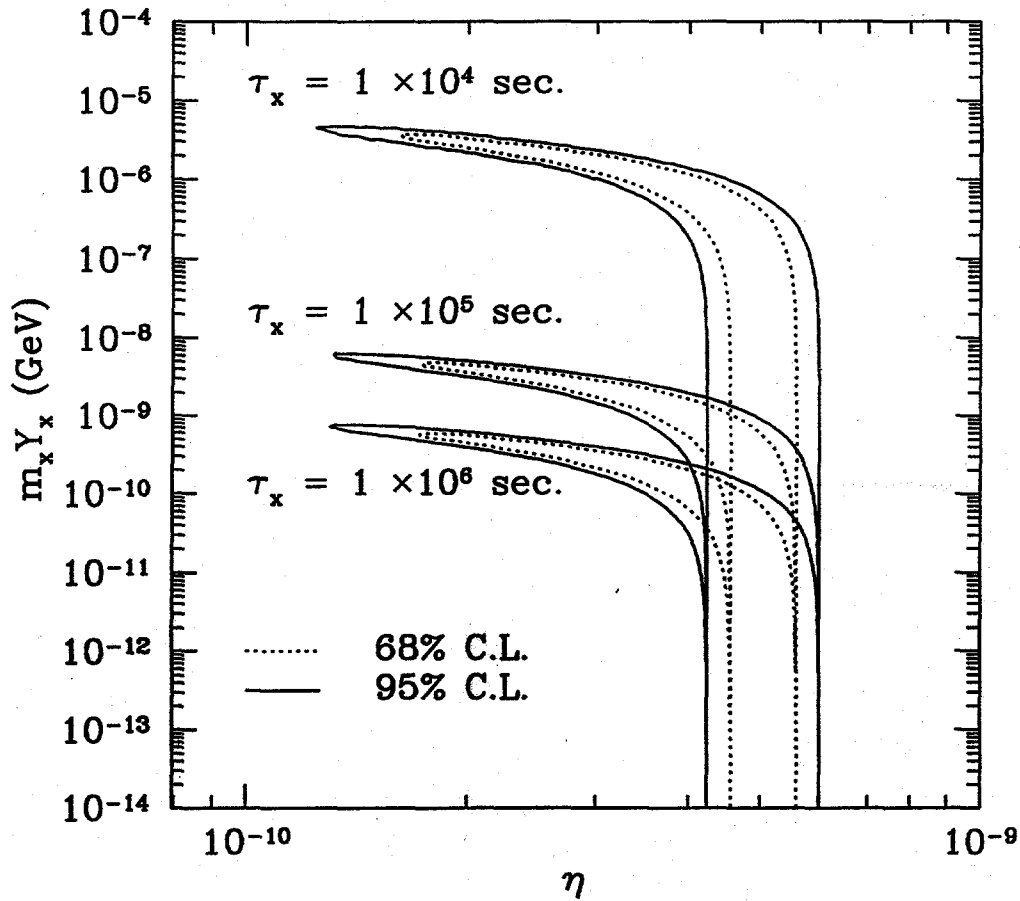
Figure 4.10: Same as Fig. 4.3, except for high value of ^{4}He and low value of D/H.
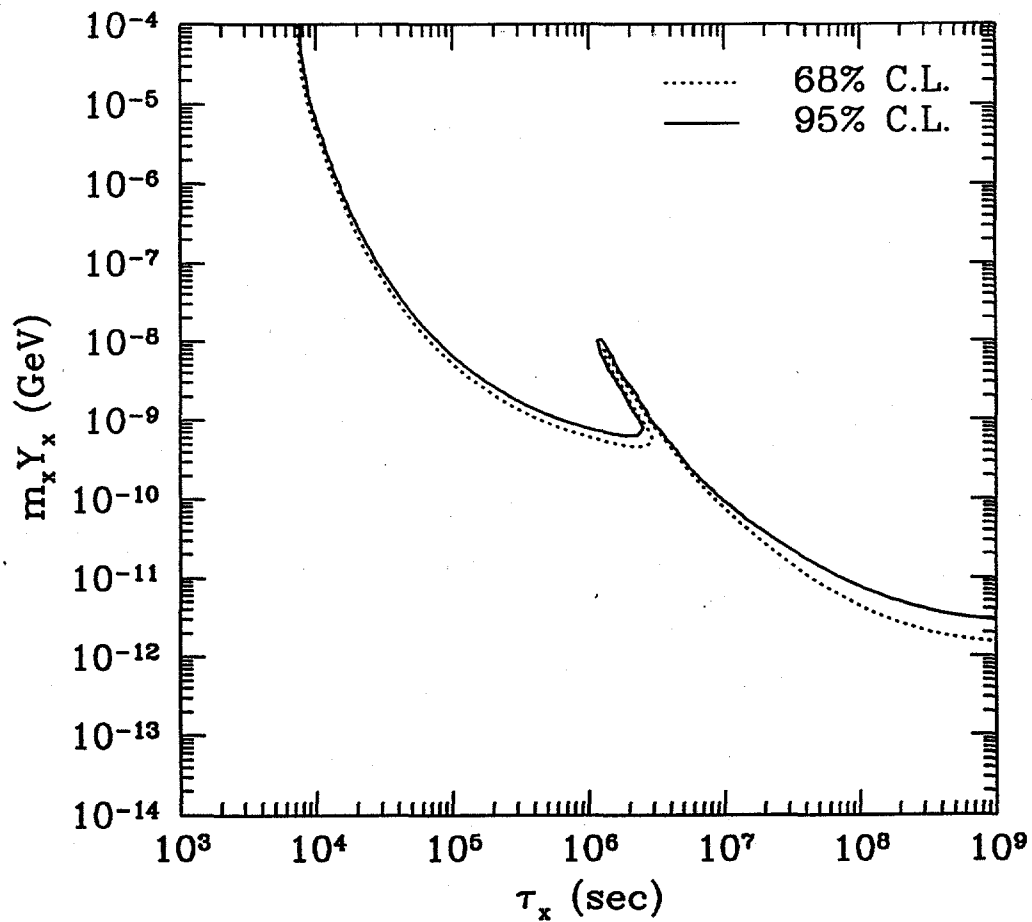
Figure 4.11: Same as Fig. 4.1, except for high value of ⁴He and high value of D/H.
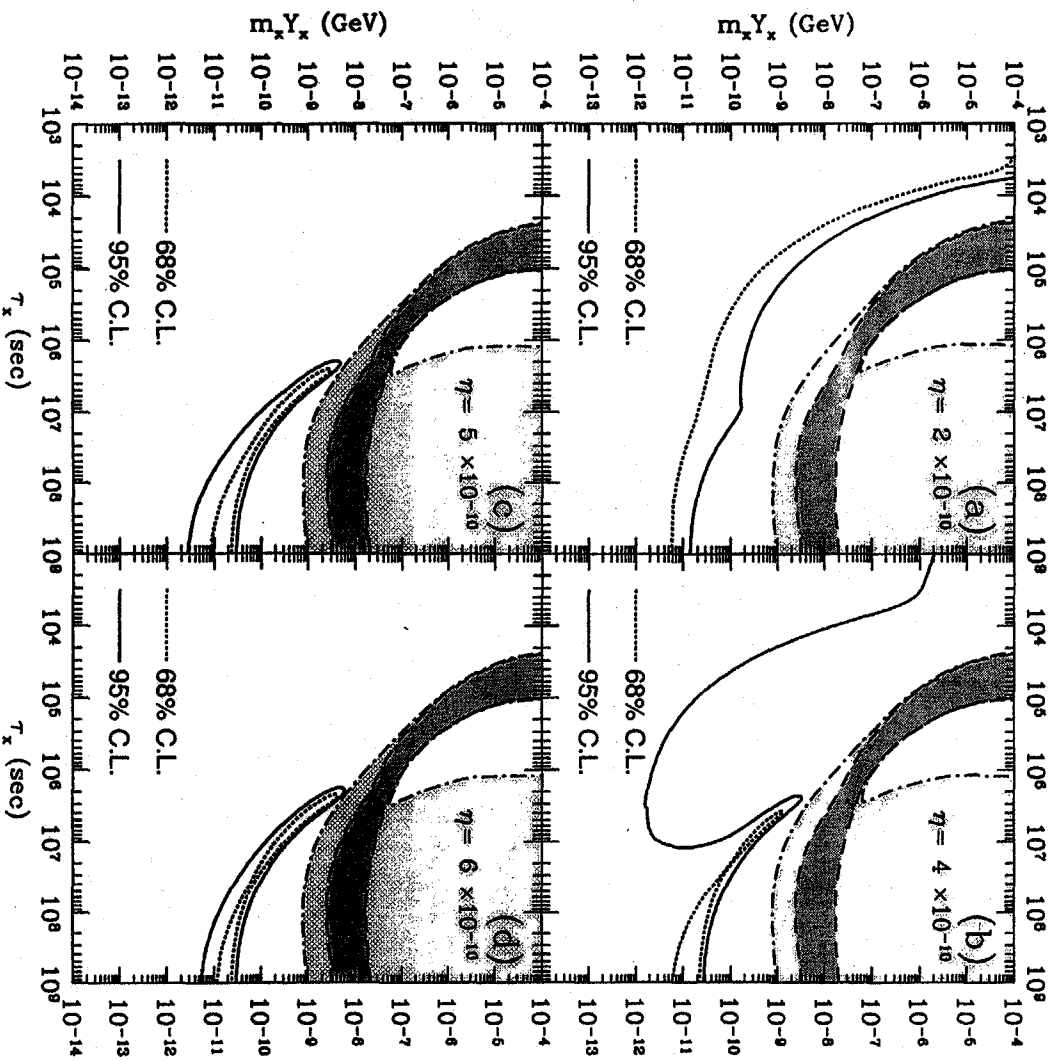
Figure 4.12: Same as Fig. 4.2, except for high value of ^{4}He and high value of D/H.
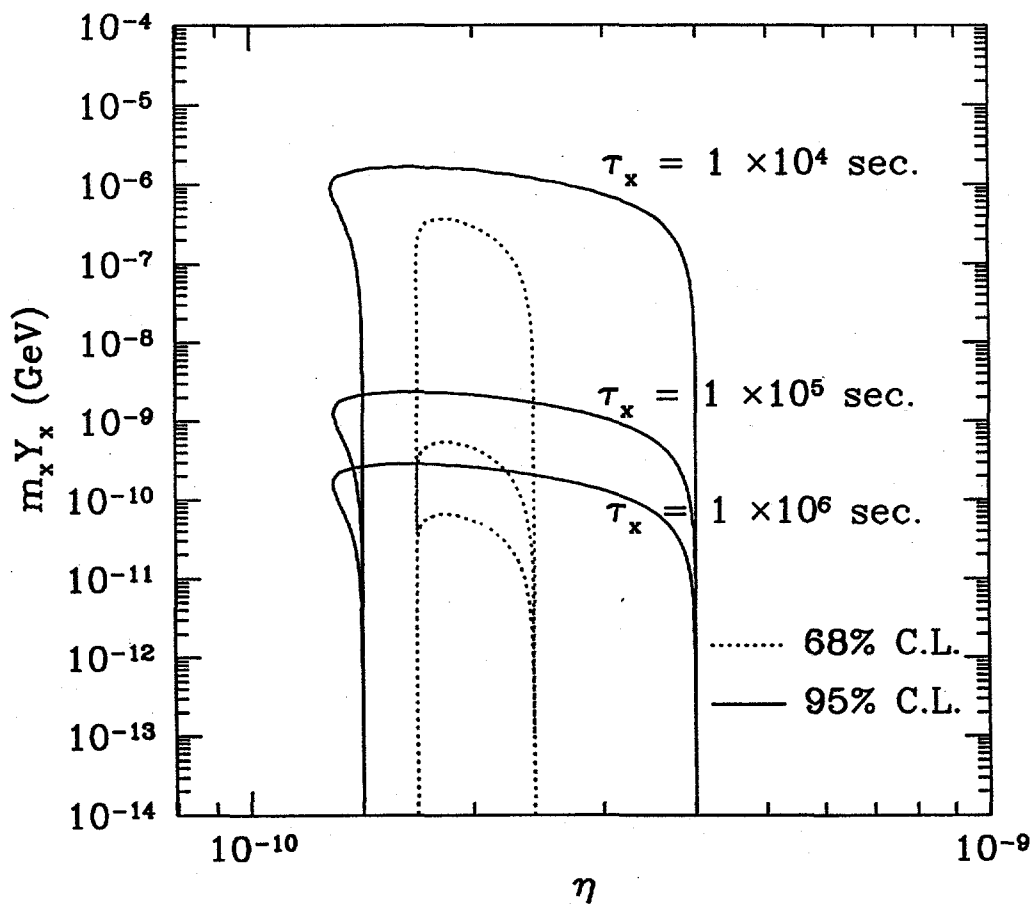
Figure 4.13: Same as Fig. 4.3, except for high value of ^{4}He and high value of D/H.
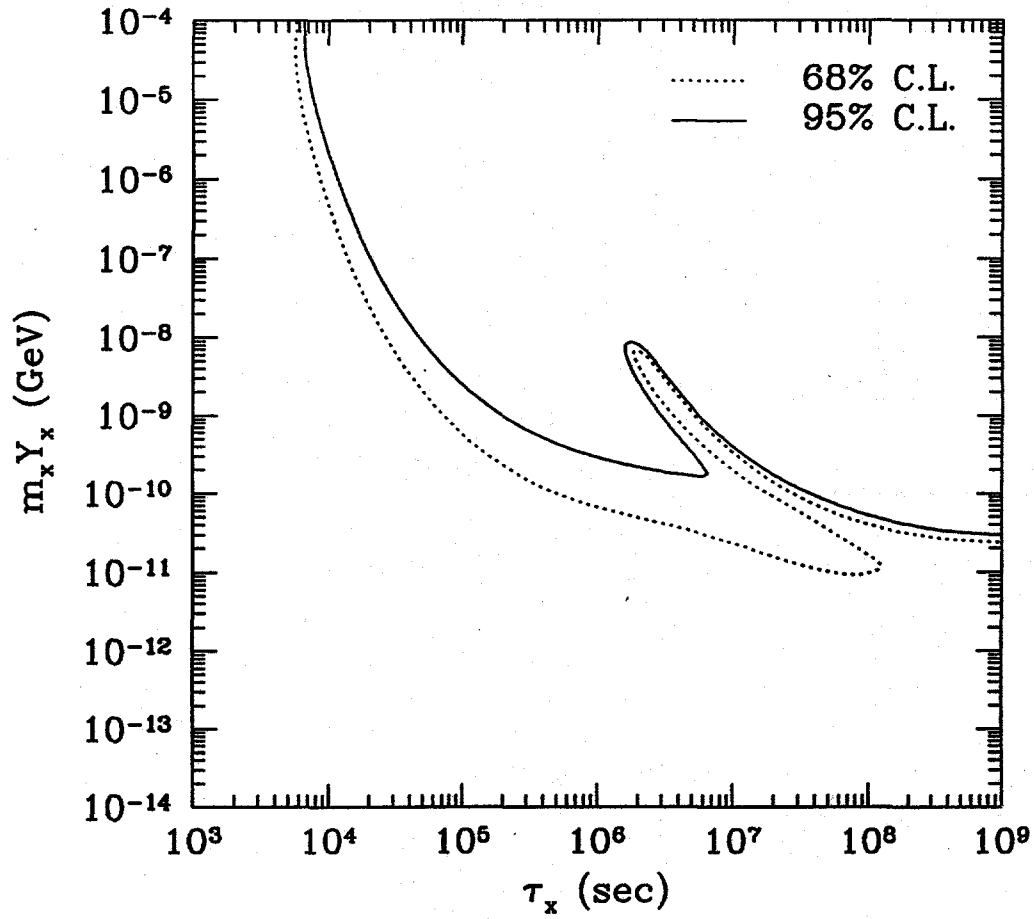
Chapter 5

Analysis Based on Proto-Solar Observations

In the preceding chapters, I have set BBN constraints on a long-lived, radiatively-decaying particle by comparing the predictions of my theory to the observed light-element abundances. I have taken my deuterium abundance from observations of highly red-shifted quasar absorption systems. However, I was not able to use ^{3}He, because there are no primordial observations of that isotope. Moreover, the existence of incompatible high and low measurements of deuterium in quasar absorption systems (QAS) casts some doubt on the QAS data.

In this chapter, I will repeat my analysis of BBN with a radiatively decaying particle. However, this time I use proto-solar and interstellar-medium (ISM) observations of D and ^{3}He (instead of QAS observations of D). Since proto-solar and ISM material is not primordial, I will have to make a few general assumptions about the chemical evolution of D and ^{3}He. In return for these assumptions, I will get another constraint (^{3}He) on the parameters $(\tau_X, m_X Y_X, \eta)$ of my theory. I begin by reviewing the proto-solar and ISM measurements of (D+^{3}He)/H and ^{3}He/H. Next, I explain how I modify my analysis to account for the chemical evolution of D and ^{3}He. Finally, I present my results (for both high and low ^{4}He, as in the previous chapter).

5.1 Proto-Solar Data on (D+^{3}He)/H and ^{3}He/H

Deuterium is very fragile, with a binding energy of just 2.2 MeV. Young stars convert all of their D to to ^{3}He through $D(p, \gamma)^3$He. Because of this, (D+^{3}He)/H is an easier quantity to evolve back in time than D/H.

In its pre–main-sequence phase, before ^{3}He began to be converted into ^{4}He, the sun was fully convective. All D was mixed down into the warmer, interior layers of the sun, where it was converted into ^{3}He. But 30 Myr before the sun became a main-sequence star, the convection zone had shrunk to its present depth, *viz.*, the outer 30% of the sun [80]. Since then, the ^{3}He/^{4}He ratio on the surface of the sun has remained constant. This ^{3}He on the surface of the sun today is the sum of the proto-solar (indicated by $\odot$) D and ^{3}He:

$$y_{23}^{\odot} \equiv y_2^{\odot} + y_3^{\odot} \tag{5.1}$$

$$= \left(\frac{n_{^4He}}{n_H}\right)_{\odot} \left(\frac{n_{^3He}}{n_{^4He}}\right)_{today}. \tag{5.2}$$

(^{3}He/^{4}He)$_{today}$ is measured in the solar wind; the proto-solar ^{4}He/H is measured in the sun's surface [81]. The resulting value for the proto-solar abundance of D and ^{3}He is [82, 12]

$$y_{23}^{\odot} = (4.09 \pm 0.92) \times 10^{-5}. \tag{5.3}$$

As can be seen in Fig. 1.2, this value (gray box) favors high η, if it is representative of the primordial value.

The proto-solar ^{3}He/H abundance is taken from trapped gases found in meteorites. One has to be careful to take the "planetary" gases, which originated in

75

the pre-solar nebula, rather than the "solar" gases, which were captured from the solar wind, and hence have been processed in the sun. I use the value [82, 12]

$$y_3^\odot = (1.52 \pm 0.34) \times 10^{-5}. \tag{5.4}$$

I have plotted the upper bound as gray arrows in Fig. 1.2, since the proto-solar value is likely to be greater than the primordial value. The figure shows that ^{3}He/H seems to exclude very small η. This is only an intuitive argument; in the next section, I describe my proper analysis that includes the joint evolution of D and ^{3}He.

In addition to the proto-solar abundances of D and ^{3}He, I will use the interstellar-medium abundance of deuterium in my analysis. This abundance is deduced through measurements of Lyman absorption lines to be [83]

$$y_2^{ism} = (1.6 \pm 0.2) \times 10^{-5}. \tag{5.5}$$

Finally, I need the primordial and proto-solar mass fractions of ^{1}H [12]:

$$X = 0.76 \pm 0.02, \tag{5.6}$$

$$X^\odot = 0.70 \pm 0.02. \tag{5.7}$$

Their ratio is

$$\alpha \equiv X^\odot/X = (0.92 \pm 0.04). \tag{5.8}$$

5.2 Proto-Solar Analysis

As in the QAS analysis in Ch. 4, I will find the confidence level at which my theoretical calculations of the abundances $\mathbf{a}^{th} = (y_2^{th}, y_3^{th}, Y^{th}, \log_{10} y_7^{th})$ agree with the abundances $\mathbf{a}^{obs} = (y_2^{obs}, y_3^{obs}, Y^{obs}, \log_{10} y_7^{obs})$ deduced from observation. The C.L. is again given by the integral (4.4) over the probability distribution function (p.d.f.) $p^\Delta(\Delta \mathbf{a})$ of the difference between the theoretical and observed abundances (see Eq. (4.2)).

Instead of making the standard assumption (as I did in Ch. 4) that the theoretical abundances are independent, here I will allow them to have a general multivariate p.d.f.:

$$p^{th}(\mathbf{a}^{th}; \bar{\mathbf{a}}^{th}, [\sigma^2]_{ij}) = \left(\frac{1}{\sqrt{2\pi}} \right)^4 \frac{1}{\sqrt{\det([\sigma^2]_{ij})}} \exp \left[-\frac{1}{2} [\mathbf{a}^{th} - \bar{\mathbf{a}}^{th}]_i [\sigma^{-2}]_{ij} [\mathbf{a}^{th} - \bar{\mathbf{a}}^{th}]_j \right],$$
(5.9)

where $[\sigma^{-2}]_{ij}$ is the inverse of the covariance matrix from Sec. 2.3.

The p.d.f. of the observed abundances is more complicated, because I need to account for the chemical evolution of D and ^{3}He. However, I can simplify the problem somewhat, because ^{4}He and ^{7}Li still have independent, Gaussian p.d.f.'s:

$$
\begin{aligned}
p^{obs}(\mathbf{a}^{obs}) &= p_{23}(y_2^{obs}, y_3^{obs}) \times \\
&\quad p_4^{Gauss}(Y^{obs}) \times p_7^{Gauss}(\log_{10} y_7^{obs}),
\end{aligned}
$$
(5.10)

where the means and standard deviations of p_4^{Gauss} and p_7^{Gauss} depend upon the parameters $\mathbf{p} = (\tau_X, m_X Y_X, \eta)$ of the theory. To find the joint p.d.f. of the primordial abundances y_2^{obs} and y_3^{obs}, I use an analysis similar to that of Hata et $al.$ [84], which is based on the chemical evolution model of Steigman and Tosi [12,

85]. First, I assume that stars convert all of their deuterium into ^{3}He. Therefore, the ratio of the proto-solar abundance of D (mass fraction $X_2^\odot$) to the primordial abundance of D (mass fraction X_2) is equal to the fraction $f \leq 1$ of gas that was never part of a star: $X_2^\odot / X_2 = f$. My second assumption is that an unknown amount of ^{3}He (primordial mass fraction X_3, proto-solar mass fraction $X_3^\odot$) is produced in stars (in excess of the D that is destroyed), and that the amount of ^{3}He that survives stellar processing and is returned to the interstellar medium is given by the "survival fraction" g_3, which is plausibly in the range [84]

$$0.25 < g_3 < 0.50. \tag{5.11}$$

This gives me a constraint on the proto-solar ^{3}He:

$$X_3^\odot \geq f X_3 + (1 - f) g_3 (X_3 + 3 X_2 / 2). \tag{5.12}$$

Thus, I derive the following constraints on the primordial abundances y_2^{obs}, y_3^{obs} of D/H and ^{3}He/H:

$$\alpha y_2^\odot \leq y_2^{obs}, \tag{5.13}$$

$$0 \geq (y_2^{obs})^2 + (y_3^{obs} - \alpha y_2^\odot - \frac{\alpha y_3^\odot}{g_3}) y_2^{obs}$$
$$+ y_3^{obs} y_2^\odot \alpha (\frac{1}{g_3} - 1), \tag{5.14}$$

where $\alpha = X^\odot / X$ is the ratio of the proto-solar and primordial mass fractions of hydrogen. Since D decreases monotonically with time, I also have

$$\alpha y_2^{ism} \leq y_2^{obs}, \tag{5.15}$$

78

where y_2^{ism} is the present-day D/H ratio in the interstellar medium.

For fixed $g_3, \alpha, y_3^\odot, y_2^{ism}$, and $y_2^\odot = y_{23}^\odot - y_3^\odot$, I assume a flat p.d.f. for y_2^{obs}, y_3^{obs}, subject to the constraints (5.13), (5.14), and (5.15). I weight these flat p.d.f.'s by a top-hat p.d.f. for g_3 (see Eq. (5.11)) and by Gaussian p.d.f.'s for $y_{23}^\odot, y_3^\odot, y_2^{ism}$, and α, where the means and standard deviations of these quantities are given in Eqs. (5.3), (5.4), (5.5), and (5.8). This gives me the p.d.f. for y_2^{obs}, y_3^{obs}.

My confidence level is now calculated for *four* degrees of freedom a_i, rather than the three degrees of freedom in Ch. 4, because of the inclusion of ^{3}He. Again, the abundances a_i^{th} are highly non-linear functions of the theory parameters $\mathbf{p} = (\tau_X, m_X Y_X, \eta)$, so it does not make sense to integrate out a theory parameter to reduce the number of degrees of freedom. Instead, I shall present my results using the same projection procedure as in the previous chapter.

5.3 Results

The proto-solar measurements of D and ^{3}He favor high η. Therefore, SBBN works well in the case of high ^{4}He, but not in the case of low SBBN. In the former case, I can place upper bounds on my model parameters, while in the latter, I investigate whether a non-standard scenario of BBN can work significantly better than SBBN.

5.3.1 Low ^{4}He ($Y^{obs} = 0.234 \pm (0.002)_{stat} \pm (0.005)_{syst}$)

Fig. 5.1 shows the 95% C.L. contour computed using four elements (D, ^{3}He,

^{4}He, and ^{7}Li). The contour is shown in the $m_X Y_X$ *vs.* τ_X plane for several representative baryon-to-photon ratios ($\eta = 2 \times 10^{-10}, 4 \times 10^{-10}, 5 \times 10^{-10}, 6 \times 10^{-10}$). The disjoint regions in Fig. 5.1a are an artifact of the low resolution of the plot; the true allowed region is a single, long, thin strip. Note that for $\eta = 6 \times 10^{-10}$, no region is allowed at the 95% C.L. Moreover, no region is allowed at the 68% C.L. for any η. As in Ch. 4, the allowed region is consistent with the constraints from ^{6}Li/^{7}Li.

Since the proto-solar data favor high η, as indicated by the gray lines in Fig. 1.2, this case is similar to that of the low QAS data (*c.f.* Fig. 4.1). In both cases, the most favored region of parameter space is at $\tau_X \lesssim 10^6$ sec, $m_X Y_X \gtrsim 10^{-10}$ GeV, and $\eta = 2$ to 4×10^{-10} (see Fig. 5.1a).

Another way to see the allowed region is in the $m_X Y_X$ *vs.* η plane at fixed τ_X, as in Fig. 5.2. The SBBN allowed range of η is shown at small $m_X Y_X$. In the proto-solar case, lower η is allowed than in the low QAS case (*c.f.* Fig. 4.2), because the uncertainty in D/H is larger. At larger $m_X Y_X$, a lower η is allowed (which produces more D and ^{3}He), because high-energy photons photodissociate D and ^{3}He. However, the upper bound on ^{3}He/H excludes $\eta \lesssim 2 \times 10^{-10}$. At still larger $m_X Y_X$, all elements are overly photodissociated.

Fig. 5.3 shows the edge of the projection of the 95% C.L. region into the $m_X Y_X$ *vs.* τ_X plane. As in Ch. 4, I project by taking the lowest C.L. value as I vary η for each (τ_X, $m_X Y_X$). In Table 5.1, I show representative values of $m_X Y_X$ that correspond to the 95% C.L. upper bound for $\tau_X = 10^4 - 10^9$ sec.

$\tau_X =$	10^4 sec	10^5 sec	10^6 sec	10^7 sec	10^8 sec	10^9 sec
95% C.L.	3×10^{-5}	1×10^{-8}	6×10^{-10}	2×10^{-13}	3×10^{-14}	$< 1 \times 10^{-14}$

Table 5.1: Upper bound on $m_X Y_X$ in units of GeV for the case of low value of ^{4}He, and proto-solar (D+^{3}He)/H and ^{3}He/H. Note that the C.L. is for four degrees of freedom, and η is varied to give the maximum values for $m_X Y_X$.

There are two main differences between the proto-solar and low QAS cases. First, because of their low binding energies, D and ^{3}He together yield a stronger constraint at high τ_X than D alone, and they exclude the "finger" in Fig. 4.3 at $\tau_X \sim 3 \times 10^6$ sec and $m_X Y_X \sim 10^{-10}$ GeV. Second, the four elements in the proto-solar case provide a stronger constraint than the three elements in the QAS case, so that no region is allowed at the 68% C.L. Thus, a radiatively decaying particle does not provide a very good solution to the "crisis" of Hata et al. [84].

5.3.2 High ^{4}He ($Y^{obs} = 0.244 \pm (0.002)_{stat} \pm (0.005)_{syst}$)

High observed ^{4}He favors high η, so it is consistent with the proto-solar (D+^{3}He)/H and ^{3}He/H in SBBN (see Fig. 1.2). This case is similar to that of high ^{4}He and low QAS D/H. Thus, I shall constrain my model parameters in this case.

In Fig. 5.4, I show the 68% and 95% C.L. contours at (a) $\eta = 2 \times 10^{-10}$, (b) $\eta = 4 \times 10^{-10}$, (c) $\eta = 5 \times 10^{-10}$, and (d) $\eta = 6 \times 10^{-10}$. Note that again, my constraints are consistent with the shaded upper bounds from ^{6}Li/^{7}Li.

I predicted that this case would be similar to that of high ^{4}He and low QAS D/H; however, Fig. 5.4 appears rather different from Fig. 4.8, especially panels

$\tau_X =$	10^4 sec	10^5 sec	10^6 sec	10^7 sec	10^8 sec	10^9 sec
95% C.L.	3×10^{-5}	6×10^{-9}	6×10^{-10}	1×10^{-12}	1×10^{-13}	$< 1 \times 10^{-14}$
68% C.L.	1×10^{-5}	3×10^{-9}	3×10^{-10}	3×10^{-13}	3×10^{-14}	$< 1 \times 10^{-14}$

Table 5.2: Same as Table 5.1, except for high ^{4}He.

(b) and (d). The proto-solar case is more easily compared to the QAS case at constant τ_X, as in Fig. 5.5. Comparing this to Fig. 4.9, one can see that in SBBN (low $m_X Y_X$), both cases favor $\eta \sim 5 \times 10^{-10}$, although the proto-solar case allows a much wider range of η. This is because the low QAS D/H value has extremely small error bars. The other main difference between the two cases is that low η is not allowed by the proto-solar data, even for the non-standard regions ($m_X Y_X \gtrsim 10^{-10}$ GeV). This is because of the upper bound on ^{3}He/H (see the gray lines in Fig. 1.2).

Fig. 5.6 shows the C.L. contours projected along the η axis into the $m_X Y_X$ vs. τ_X plane. Note that the combination of (D+^{3}He)/H and ^{3}He/H provides a strong bound at long lifetimes and forbids a "finger" near the center of the plot (c.f. Fig. 4.10). Table 5.2 gives the 68% and 95% C.L. upper bounds on $m_X Y_X$ for various of τ_X.

As I discussed in Section 4.3, the blackbody spectrum of the cosmic microwave background radiation imposes an additional constraint on X, for lifetimes τ_X longer than 10^6 sec (see Eqn (4.8)). However, the CMBR constraint is not as strong as the limits set by the combination of (D+^{3}He)/H and ^{3}He/H for both high and low ^{4}He. Hadronic decays of X would lead to stricter constraints on the

82

model parameters $m_X Y_X$, τ_X, and η, because hadronic showers lead to efficient

production of the light elements.

Figure 5.1: 95% C.L. in the $m_X Y_X$ vs. τ_X plane, for low value of ^{4}He, and proto-solar $(D+^3He)/H$ and $^3He/H$. The allowed regions lie (a) inside the contours, and (b,c) below and to the left of the contours. I take (a) $\eta = 2 \times 10^{-10}$, (b) $\eta = 4 \times 10^{-10}$, (c) $\eta = 5 \times 10^{-10}$, and (d) $\eta = 6 \times 10^{-10}$. The shaded regions are $y_6/y_7 \gtrsim 0.5$, and the darker shaded regions are $y_6/y_7 \gtrsim 1.3$.
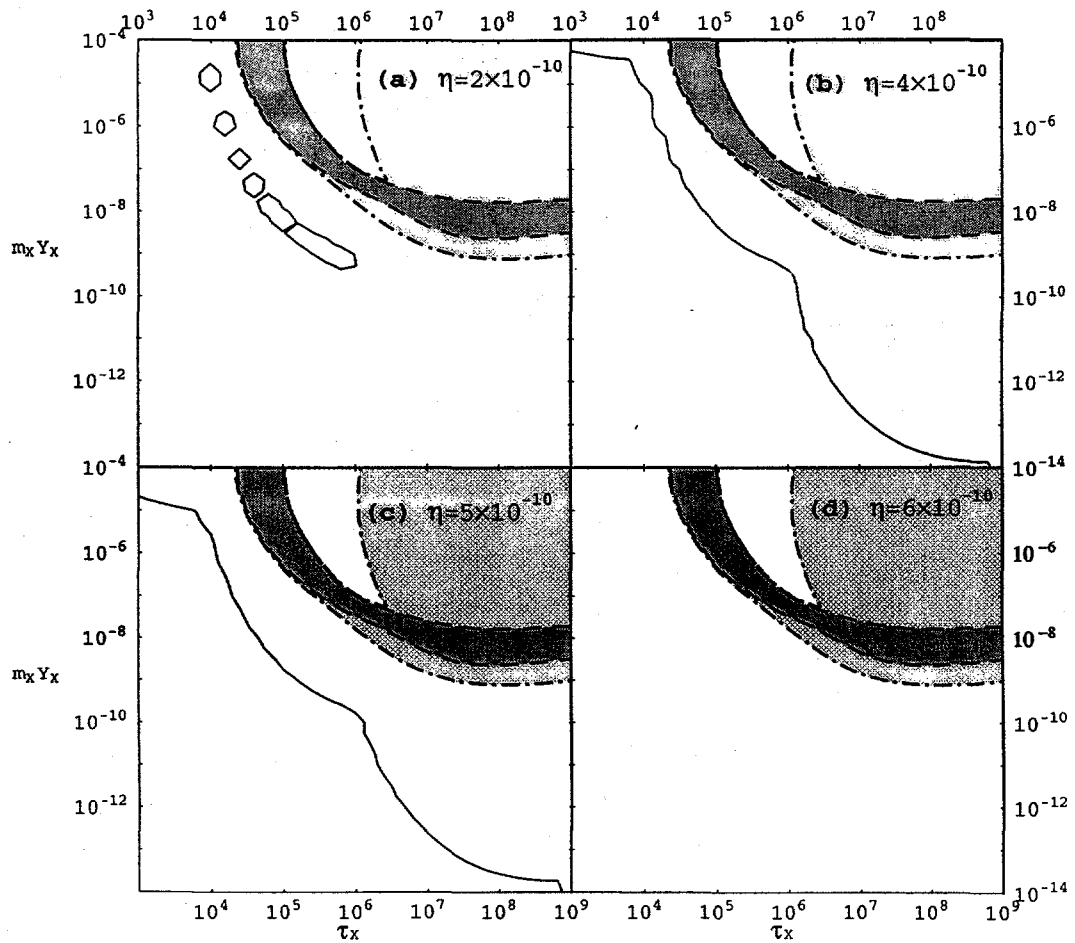
Figure 5.2: 95% C.L. in the $m_X Y_X$ vs. η plane for various values of τ_X, for low value of ^{4}He, and proto-solar (D+^{3}He)/H and ^{3}He/H. The allowed regions lie within the contours.
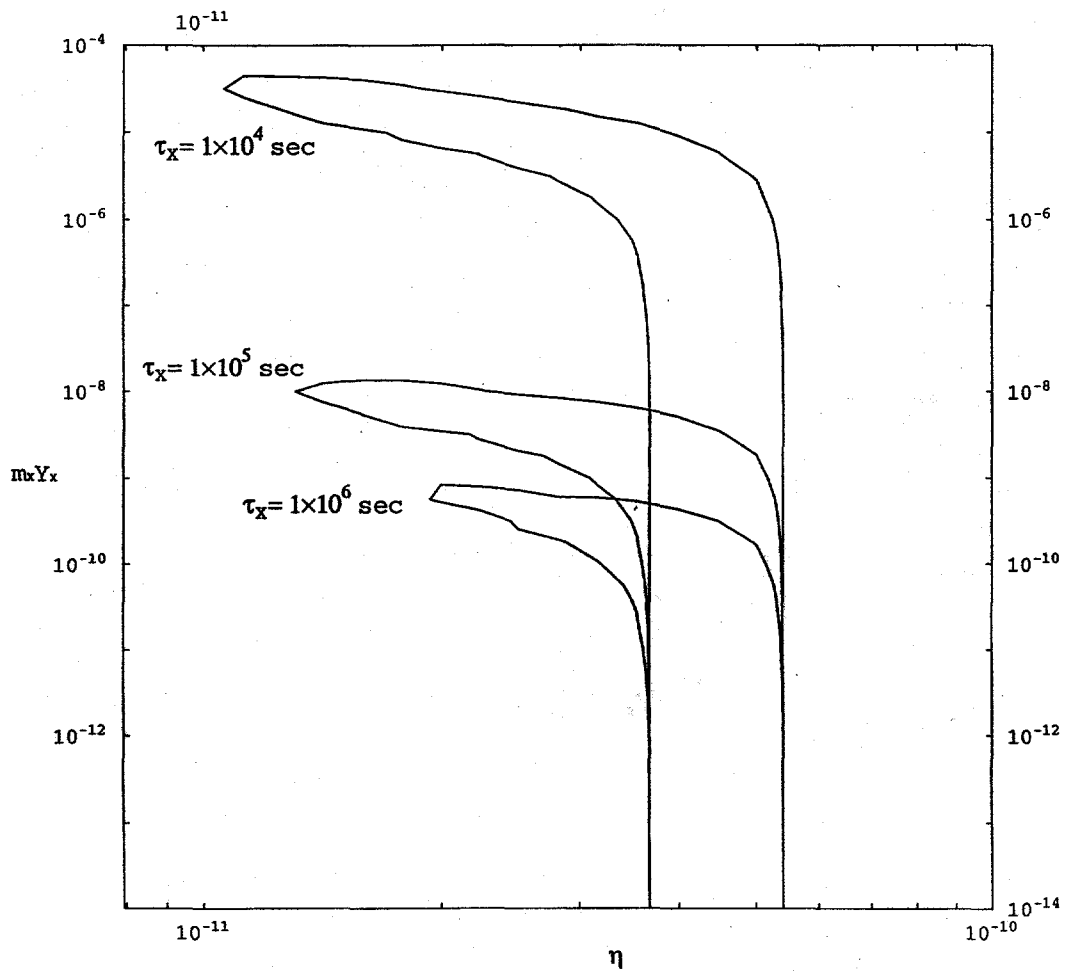
Figure 5.3: 95% C.L. contour projected along the η axis, for low value of ^{4}He, and proto-solar $(D+^3He)/H$ and $^3He/H$. The allowed region lies below and to the left of the contour.
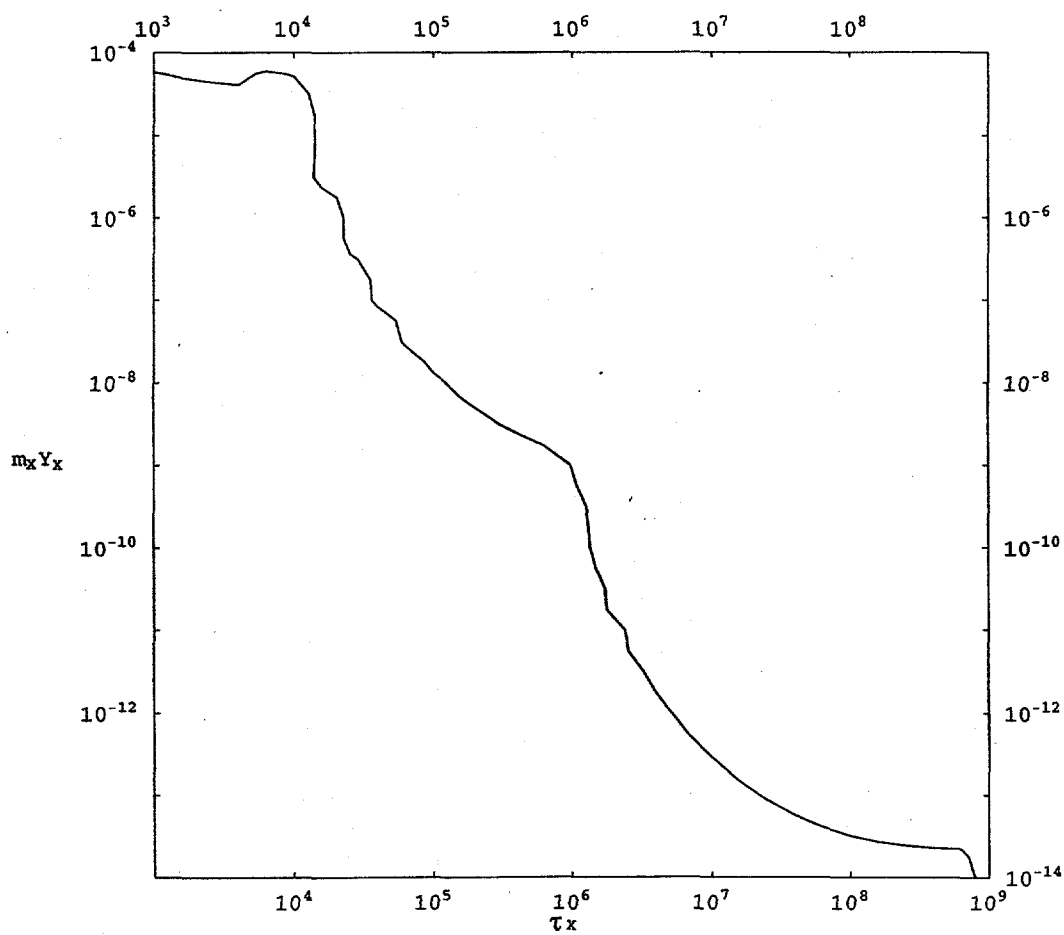
Figure 5.4: Same as Fig. 5.1, except for high value of ^{4}He. The solid line is the 95% C.L.; the dotted line is the 68% C.L.
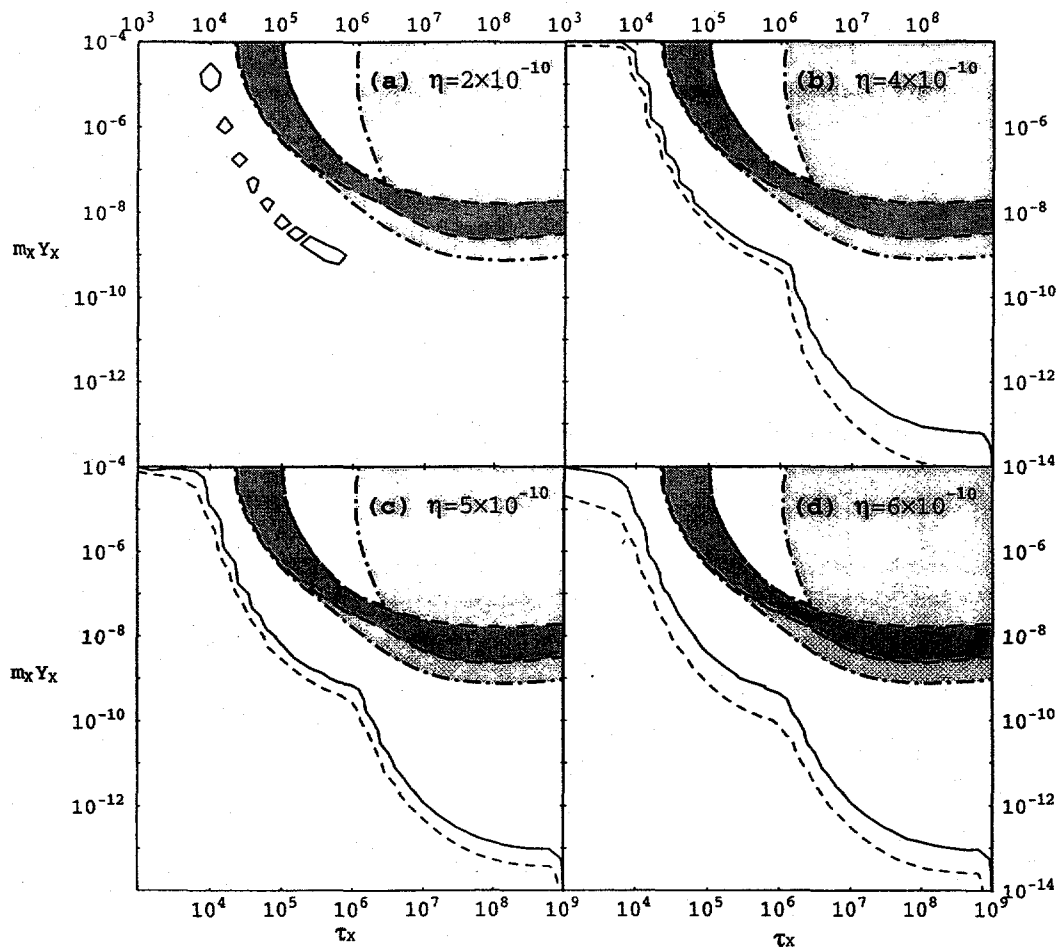
Figure 5.5: Same as Fig. 5.2, except for high value of ^{4}He. The solid line is the 95% C.L.; the dotted line is the 68% C.L.
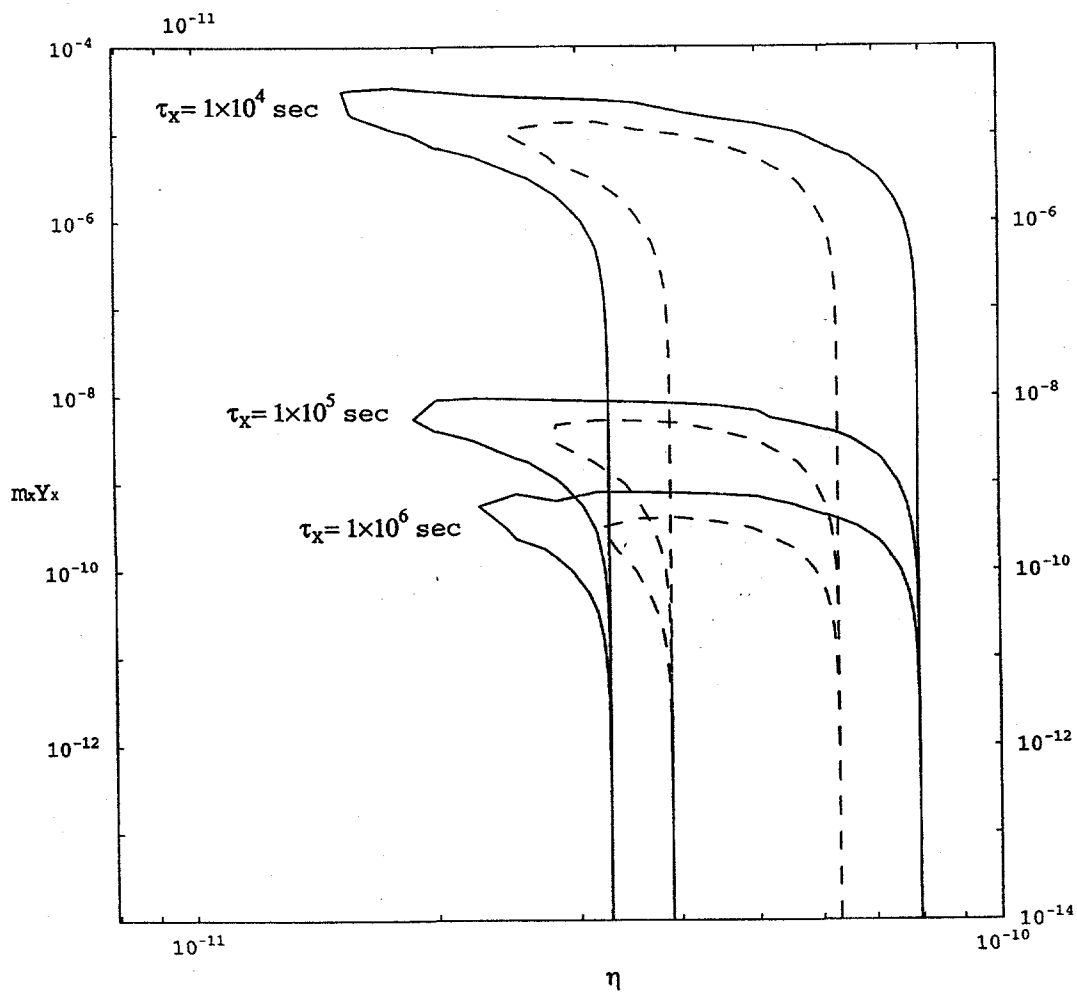
Figure 5.6: Same as Fig. 5.3, except for high value of ^{4}He. The solid line is the 95% C.L.; the dotted line is the 68% C.L.
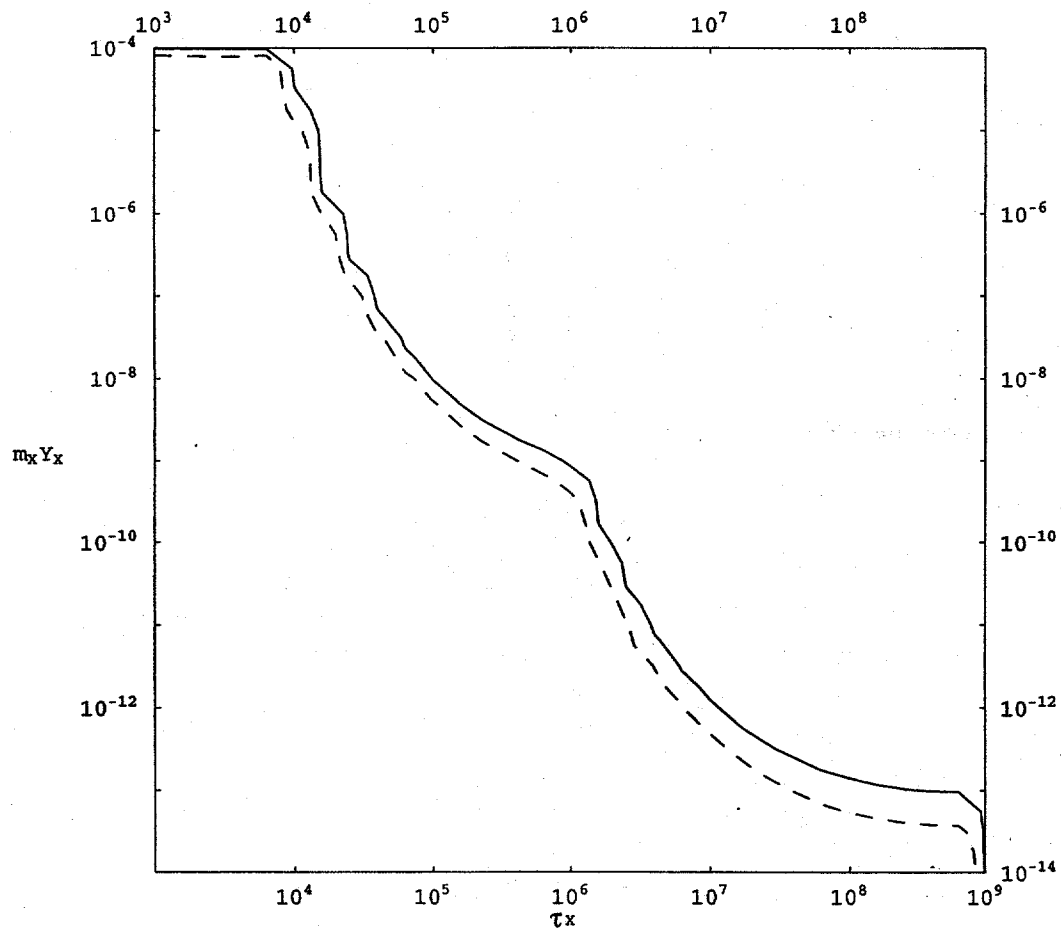
Chapter 6

Models

So far, I have discussed general constraints from BBN on radiatively decaying particles. In the minimal standard model, there is no such particle. However, some extensions of the standard model naturally result in such exotic particles, and the light-element abundances may be affected significantly in these cases. In this section, I present several examples of such radiatively decaying particles, and discuss the constraints.

In particular, I will consider particles in supergravity models [86]. Global supersymmetry (SUSY), a symmetry between fermions and bosons, is attractive because it can solve the gauge hierarchy problem (*viz.*, how the electroweak scale can be so much smaller than the Planck scale, despite renormalization). Supersymmetry solves this problem because positive contributions from bosonic loop integrals are precisely canceled by negative contributions from the corresponding fermionic loop integrals. When SUSY is gauged, it automatically includes gravity; hence, local supersymmetry is known as "supergravity."

6.1 Gravitino

My first example of a long-lived particle is the gravitino ψ, which appears in

all the supergravity models. The gravitino is the superpartner of the graviton, and its interactions are suppressed by inverse powers of the reduced Planck scale $M_* \simeq 2.4 \times 10^{18}$ GeV [87]. Because of this suppression, the lifetime of the gravitino is very long. Assuming that the gravitino's dominant decay mode is to a photon and its superpartner (the photino), the gravitino's lifetime is given by

$$\tau_{3/2} \simeq \frac{8\pi M_*^2}{m_{3/2}^3} \simeq 4 \times 10^5 \text{ sec} \times (m_{3/2}/1 \text{ TeV})^{-3}, \qquad (6.1)$$

where $m_{3/2}$ is the gravitino mass. Notice that the gravitino mass is $O(100 \text{ GeV} - 1 \text{ TeV})$ in models in which SUSY breaking is communicated by gravity from a hidden sector to the SUSY sector. Such a mass for the gravitino results in a lifetime that may affect the primordial light-element abundances.

If the gravitino is in thermal equilibrium in the early universe, then its energy density is of order T^4, as given in Eq. (1.16). If the gravitino is not diluted, then it matter-dominates the universe when the temperature falls below $m_{3/2}$. This completely spoils the (near) success of BBN theory. Usually, this problem is solved by introducing inflation, which dilutes away the primordial gravitinos. After reheating at the end of inflation, a smaller number of gravitinos are produced through the scattering processes of thermal particles. The abundance $Y_{3/2} = n_{3/2}/n_\gamma$ of gravitinos depends on the reheating temperature T_R, and is given by [8]

$$Y_{3/2} \simeq 3 \times 10^{-11} \times (T_R/10^{10} \text{ GeV}). \qquad (6.2)$$

Therefore, if the reheating temperature is too high, then gravitinos are overproduced, and too many light nuclei are photodissociated when the gravitinos decay.

91

My constraints on $(\tau_X, m_X Y_X)$ from Chapters 4 and 5 can be transformed into constraints on $(m_{3/2}, T_R)$. In Figures 6.1 and 6.2, I show the transformations of the projected 95% C.L. boundaries from Figs. 4.3, 4.7, 4.10, 4.13, 5.3, and 5.6. The proto-solar data yield tighter constraints on T_R for all $m_{3/2}$ than the QAS data, particularly at low $m_{3/2}$ (long lifetimes). For several values of the gravitino mass, I quote the most conservative (*i.e.*, weakest) upper bound on the reheating temperature from Figs. 6.1 and 6.2:

$$m_{3/2} = 100 \text{ GeV} \quad (\tau_{3/2} \simeq 4 \times 10^8 \text{ sec}) \quad : \quad T_R \lesssim 3 \times 10^8 \text{ GeV},$$

$$m_{3/2} = 1 \text{ TeV} \quad (\tau_{3/2} \simeq 4 \times 10^5 \text{ sec}) \quad : \quad T_R \lesssim 1 \times 10^9 \text{ GeV},$$

$$m_{3/2} = 3 \text{ TeV} \quad (\tau_{3/2} \simeq 1 \times 10^4 \text{ sec}) \quad : \quad T_R \lesssim 3 \times 10^{11} \text{ GeV}.$$

If the gravitino is heavy enough ($m_{3/2} \gtrsim 5$ TeV), then its lifetime is too short to destroy even D. In this case, my only constraint is from the overproduction of ^{4}He. If the gravitino mass is lighter, then the lifetime is long enough to destroy D or even ^{4}He. In this case, my constraint on the reheating temperature is more severe.

6.2 Bino

Another example of my decaying particle is the lightest superparticle in the minimal supersymmetric standard model (MSSM) sector[1], if it is heavier than the gravitino. In many theories, the lightest superparticle is the "neutralino"—a

---

[1] The MSSM consists of the standard model particles, their superpartners, two Higgs bosons, and their superpartners.

linear combination of the superpartners of the photon, Z boson, and Higgs bosons. In these theories, the lightest neutralino can decay into a high-energy photon and a gravitino. Thus, I may use BBN to constrain the MSSM.

The abundance (1.20) of the lightest neutralino is determined by the temperature T_F at which it freezes out of the thermal bath. In a theory with heavier sfermions[2], the neutralino (mass m) has a smaller annihilation cross section σ, so it freezes out at a higher temperature (when the annihilation rate falls below the expansion rate: $\sigma(mT_F)^{3/2}\exp(-m/T_F) \sim \Gamma \lesssim H \sim T_F^2/M_*$), with a higher thermal abundance. Thus, the upper bound on $m_X Y_X$ can be translated into an upper bound on the mass scale of the sfermions.

In order to investigate this scenario, I consider the simplest case where the lightest neutralino is (almost) purely bino $\tilde{B}$ (the superpartner of the $U(1)$ gauge boson B). In this case, the lightest neutralino pair-annihilates through squark and slepton exchange. In particular, if the right-handed sleptons are the lightest sfermions, then the dominant annihilation is $\tilde{B} + \tilde{B} \rightarrow l^+ + l^-$. The annihilation cross section of this process is given by [88]

$$\langle \sigma v_{\rm rel} \rangle = 8\pi\alpha_1^2\langle v^2 \rangle \left\{ \frac{m_{\tilde{B}}^2}{(m_{\tilde{B}}^2 + m_{l_R}^2)^2} - \frac{2m_{\tilde{B}}^4}{(m_{\tilde{B}}^2 + m_{l_R}^2)^3} + \frac{2m_{\tilde{B}}^6}{(m_{\tilde{B}}^2 + m_{l_R}^2)^4} \right\}, \quad (6.3)$$

where $\langle v^2 \rangle$ is the thermal average of the square of the velocity of the bino, and I have added the contributions from all three generations by assuming that the

---

[2]Squarks, sleptons, and sfermions are the respective superpartners of the quarks, leptons, and standard model fermions.

right-handed sleptons are degenerate.[3] With this annihilation cross section, the Boltzmann equation for the number density of binos is given by

$$\dot{n}_{\tilde{B}} + 3Hn_{\tilde{B}} = -2\langle\sigma v_{\mathrm{rel}}\rangle(n_{\tilde{B}}^2 - (n_{\tilde{B}}^{\mathrm{EQ}})^2),\tag{6.4}$$

where $n_{\tilde{B}}^{\mathrm{EQ}}$ is the equilibrium number density of binos. The factor 2 is present because two binos annihilate into leptons in each interaction. I solved this equation and obtained the mass density of the bino as a function of the bino mass and the right-handed slepton mass. (For details, see e.g., Ref. [14]). Numerically, for $m_{\tilde{B}} = 100$ GeV, $m_X Y_X$ ranges from $\sim 10^{-9}$ GeV to $\sim 10^{-5}$ GeV as I vary $m_{\tilde{l}_R}$ from 100 GeV to 1 TeV. If $m_X Y_X$ is in this range, the primordial light-element abundances are affected significantly, unless the lifetime of the bino is shorter than $10^4 - 10^5$ sec (see Figs. 2.2 – 2.6). The lifetime of the bino is given by

$$\tau_{\tilde{B}} = \left[\frac{1}{48\pi}\frac{m_{\tilde{B}}^5\cos^2\theta_{\mathrm{W}}}{m_{3/2}^2 M_*^2}\right]^{-1} \simeq 7\times10^4 \ \sec\times\left(\frac{m_{\tilde{B}}}{100 \ \mathrm{GeV}}\right)^{-5}\left(\frac{m_{3/2}}{1 \ \mathrm{GeV}}\right)^2.\tag{6.5}$$

Notice that the lifetime becomes shorter as the gravitino mass decreases; hence, too much D and ^{7}Li are destroyed if the gravitino mass is too large. The constraints given in Figs. 4.3, 4.7, 4.10, 4.13, 5.3, and 5.6 therefore become upper bounds on the gravitino mass. Since the abundance of the bino is an increasing function of the slepton mass $m_{\tilde{l}_R}$, the upper bound on the gravitino mass is more severe for larger slepton masses. For example, for $m_{\tilde{B}} = 100$ GeV, the upper bounds on the gravitino mass are shown in Fig. 6.3 and Fig. 6.4. For all values of the

---

[3]If the bino is heavier than the top quark, then the s-wave contribution annihilating into top quarks becomes important. In this work, I do not consider this case.

slepton mass, the QAS data give a much stronger constraint than the proto-solar data. For some representative values of the slepton mass, the most conservative constraints are:

$$m_{\tilde{l}_R} = 100 \text{ GeV} \quad : \quad m_{3/2} \lesssim 4 \text{ GeV},$$

$$m_{\tilde{l}_R} = 300 \text{ GeV} \quad : \quad m_{3/2} \lesssim 2 \text{ GeV},$$

$$m_{\tilde{l}_R} = 1 \text{ TeV} \quad : \quad m_{3/2} \lesssim 700 \text{ MeV}.$$

As expected, for a larger value of the slepton mass, the primordial abundance of the bino gets larger, and the upper bound on the gravitino mass becomes smaller.

6.3   Modulus

Another interesting source of high-energy photons is a modulus field ϕ. Moduli are massless scalars that arise in string-inspired supergravity theories due the compactification of extra spatial dimensions. A modulus field acquires mass from SUSY breaking. In many models, the modulus mass m_ϕ is of the same order as the gravitino mass (see for example [89]); with such a mass, the modulus is a candidate for my long-lived, massive X particle.

The equation of motion of a modulus with a simple quadratic potential in an expanding universe follows from conservation of energy-stress $T^\mu{}_{\nu;\mu} = 0$ [14]:

$$\ddot{\phi} + 3H\dot{\phi} + \Gamma_\phi\dot{\phi} + m_\phi^2\phi = 0 \tag{6.6}$$

In the early universe, the mass of the modulus field is negligible compared to the expansion rate of the universe. Thus, the modulus field is a strongly-overdamped

harmonic oscillator, so the modulus amplitude may sit far from the minimum of its potential. Since the only scale parameter in supergravity is the Planck scale M_*, the initial amplitude ϕ_0 is naively expected to be of $O(M_*)$. However, this initial amplitude is too large; the modulus would matter-dominate the universe, and photons from its decay would distort the spectrum of the cosmic microwave background radiation. In this model, I regard ϕ_0 as a free parameter on which I can set an upper bound.

Once the expansion rate becomes smaller than the mass of the modulus field, the modulus field begins to oscillate. Assuming homogeneity, the energy density and pressure are

$$\rho_\phi = \frac{1}{2}\dot{\phi}^2 + \frac{m^2}{2}\phi^2 \tag{6.7}$$

$$p_\phi = \frac{1}{2}\dot{\phi}^2 - \frac{m^2}{2}\phi^2 \tag{6.8}$$

The average of the pressure over a period is zero; the average of the energy density is $\langle\dot{\phi}^2\rangle$, so the averaged energy density evolves as

$$\dot{\rho}_\phi + 3H\rho_\phi + \Gamma_\phi\rho_\phi = 0. \tag{6.9}$$

Therefore, ρ_ϕ red-shifts as a^{-3} (where a is the scale factor), and the oscillating modulus behaves as non-relativistic matter. The modulus eventually decays when the expansion rate becomes comparable to its decay rate

$$\Gamma_\phi = \frac{1}{\tau_\phi} \simeq \frac{m_{3/2}^3}{8\pi M_*^2} \simeq \frac{1}{4 \times 10^5 \text{ sec}} \times \left(\frac{m_{3/2}}{1 \text{ TeV}}\right)^3. \tag{6.10}$$

Without entropy production from another source, the modulus density at the

96

decay time is approximately

$$m_\phi Y_\phi = \frac{\rho_\phi}{n_\gamma} \sim 5 \times 10^{10} \text{ GeV} \times (m_\phi/1 \text{ TeV})^{1/2}(\phi_0/M_*)^2. \tag{6.11}$$

As in my other models, I can convert my constraints on $(\tau_X, m_X Y_X)$ (Figs. 4.3, 4.7, 4.10, 4.13, 5.3, and 5.6) into constraints on (m_ϕ, ϕ_0). For small $m_{3/2}$ (long lifetimes), the proto-solar data give a tighter constraint, because too much ^{3}He is dissociated. But for higher masses, the QAS data give a slightly stronger constraint. Using the most conservative of these 95% C.L. constraints from Figs. 6.5 and Figs. 6.6, I still obtain very stringent bounds on the initial amplitude of the modulus field ϕ_0:

$$m_\phi = 100 \text{ GeV} \quad (\tau_\phi \sim 4 \times 10^8 \text{ sec}) \quad : \quad \phi_0 \lesssim 1 \times 10^8 \text{ GeV},$$

$$m_\phi = 1 \text{ TeV} \quad (\tau_\phi \sim 4 \times 10^5 \text{ sec}) \quad : \quad \phi_0 \lesssim 5 \times 10^8 \text{ GeV},$$

$$m_\phi = 3 \text{ TeV} \quad (\tau_\phi \sim 1 \times 10^4 \text{ sec}) \quad : \quad \phi_0 \lesssim 2 \times 10^{10} \text{ GeV}.$$

Clearly, my upper bound from BBN rules out the naive expectation that $\phi_0 \sim M_*$. It is important to notice that (conventional) inflation cannot solve this difficulty by diluting the coherent mode of the modulus field. This is because the expansion rate of the universe is usually much larger than the mass of the modulus field, so the modulus field has not yet begun to oscillate. Thus, the modulus has constant amplitude and energy density throughout an early inflationary epoch. One attractive solution is a thermal inflation model proposed by Lyth and Stewart [90]. In the thermal inflation model, a late mini-inflation of about 10 e-folds reduces the modulus density. Even if thermal inflation occurs, there may remain a significant

modulus energy density that decays to high-energy photons. Thus, BBN gives a stringent constraint on the thermal inflation model.

Figure 6.1: Contours of 95% C.L., yielding an upper bound on the reheating temperature, as a function of the gravitino mass. QAS data are used for the observed D/H ratio.
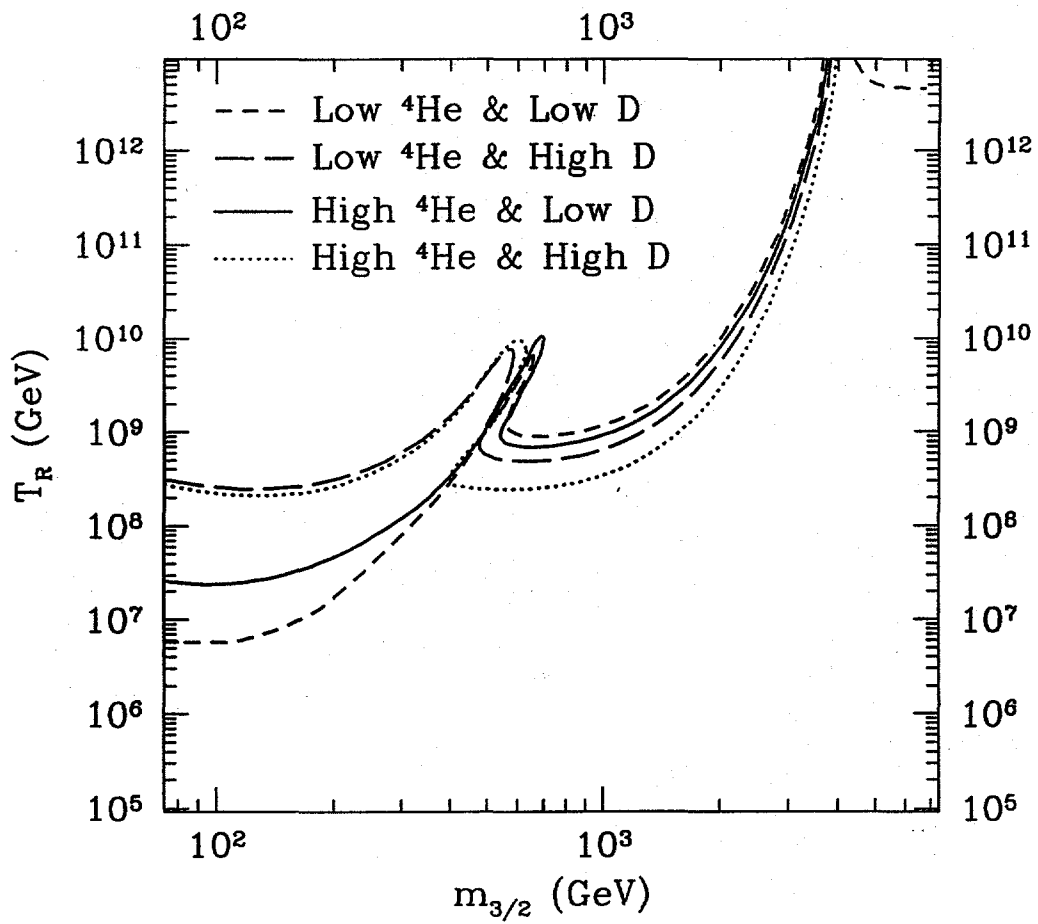
Figure 6.2: Contours of 95% C.L., yielding an upper bound on the reheating temperature, as a function of the gravitino mass. Proto-solar data are used for the observed D/H and $(D+^3He)/H$ ratios.
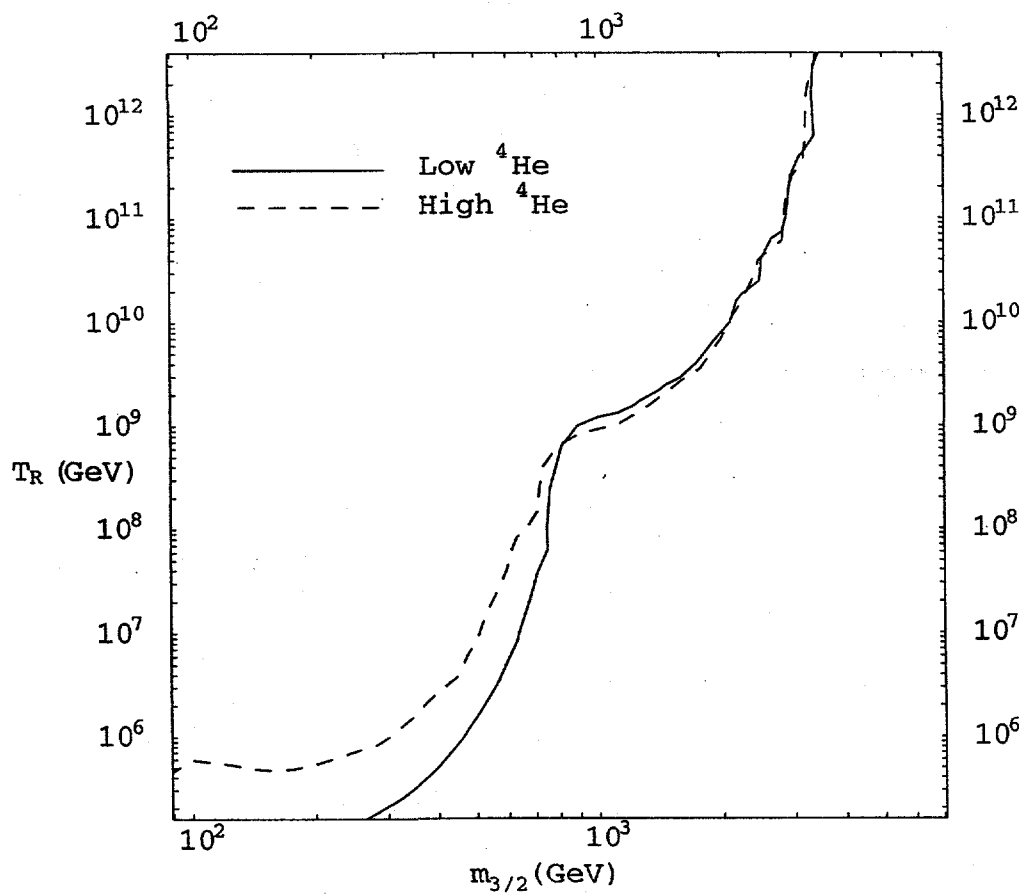
Figure 6.3: Contours of 95% C.L., yielding an upper bound on the gravitino mass, as a function of the right-handed slepton mass. QAS data are used for the observed D/H ratio.
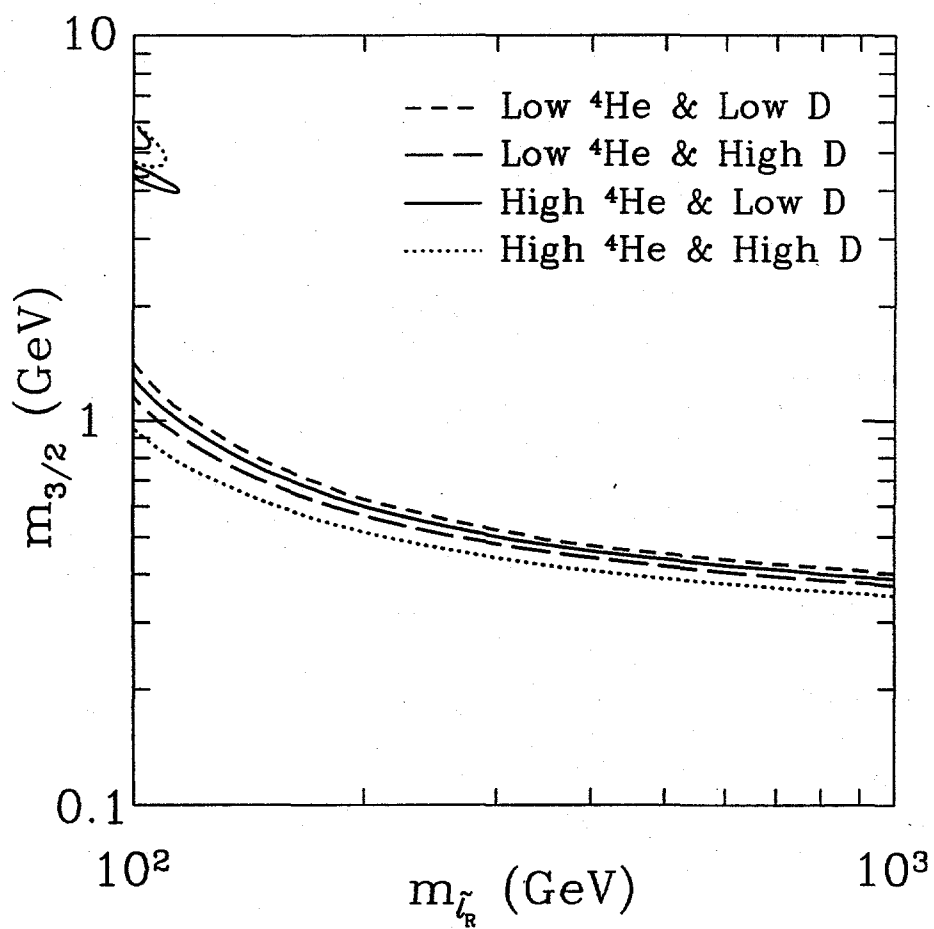
Figure 6.4: Contours of 95% C.L., yielding an upper bound on the gravitino mass, as a function of the right-handed slepton mass. Proto-solar data are used for the observed D/H and $(D+^3He)/H$ ratios.
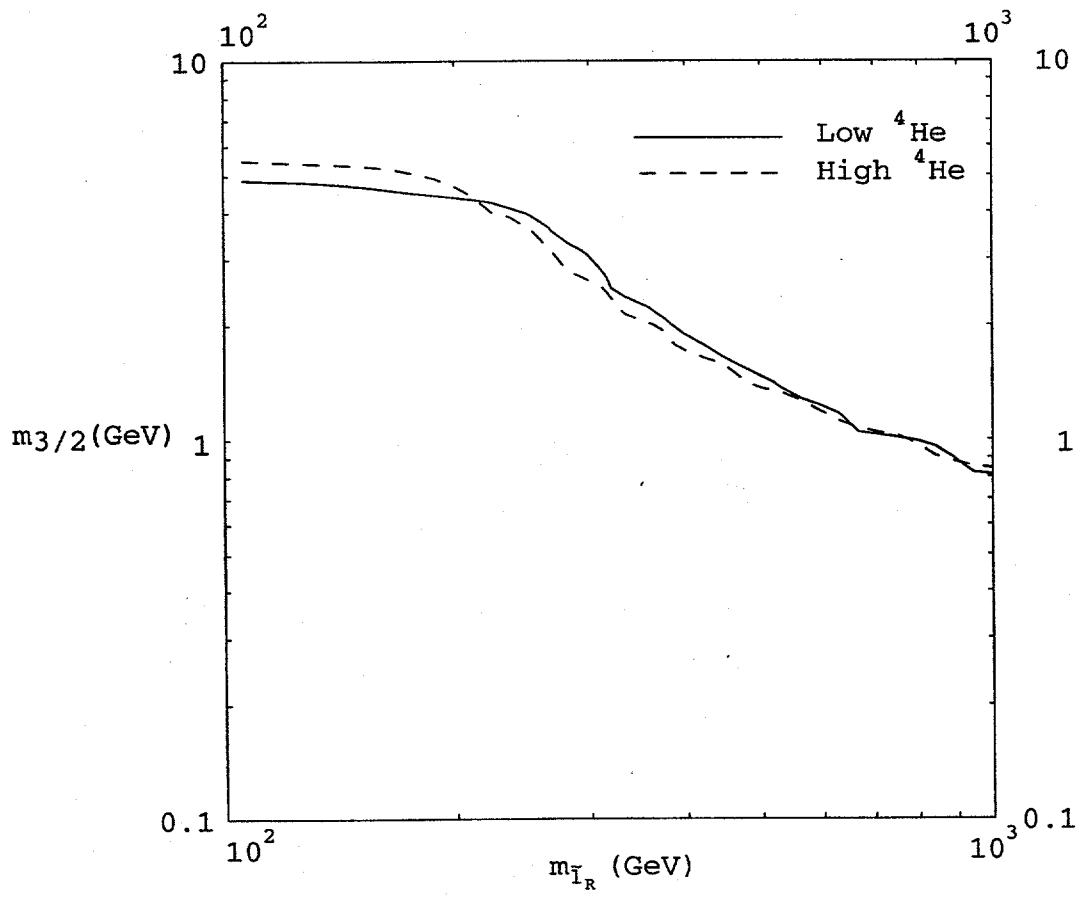
Figure 6.5: Contours of 95% C.L., yielding an upper bound on the the initial modulus amplitude ϕ_0, as a function of the modulus mass. QAS data are used for the observed D/H ratio.
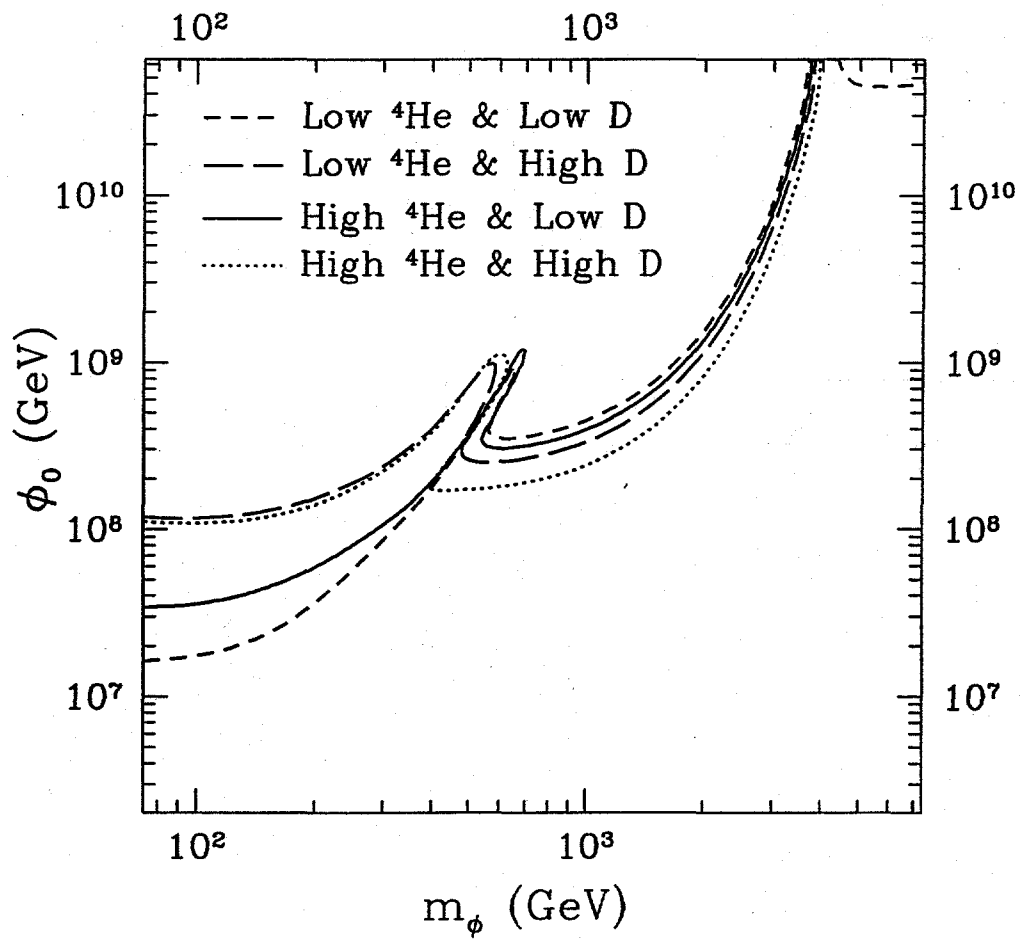
Figure 6.6: Contours of 95% C.L., yielding an upper bound on the the initial modulus amplitude ϕ_0, as a function of the modulus mass. Proto-solar data are used for the observed D/H and $(D+^3He)/H$ ratios.
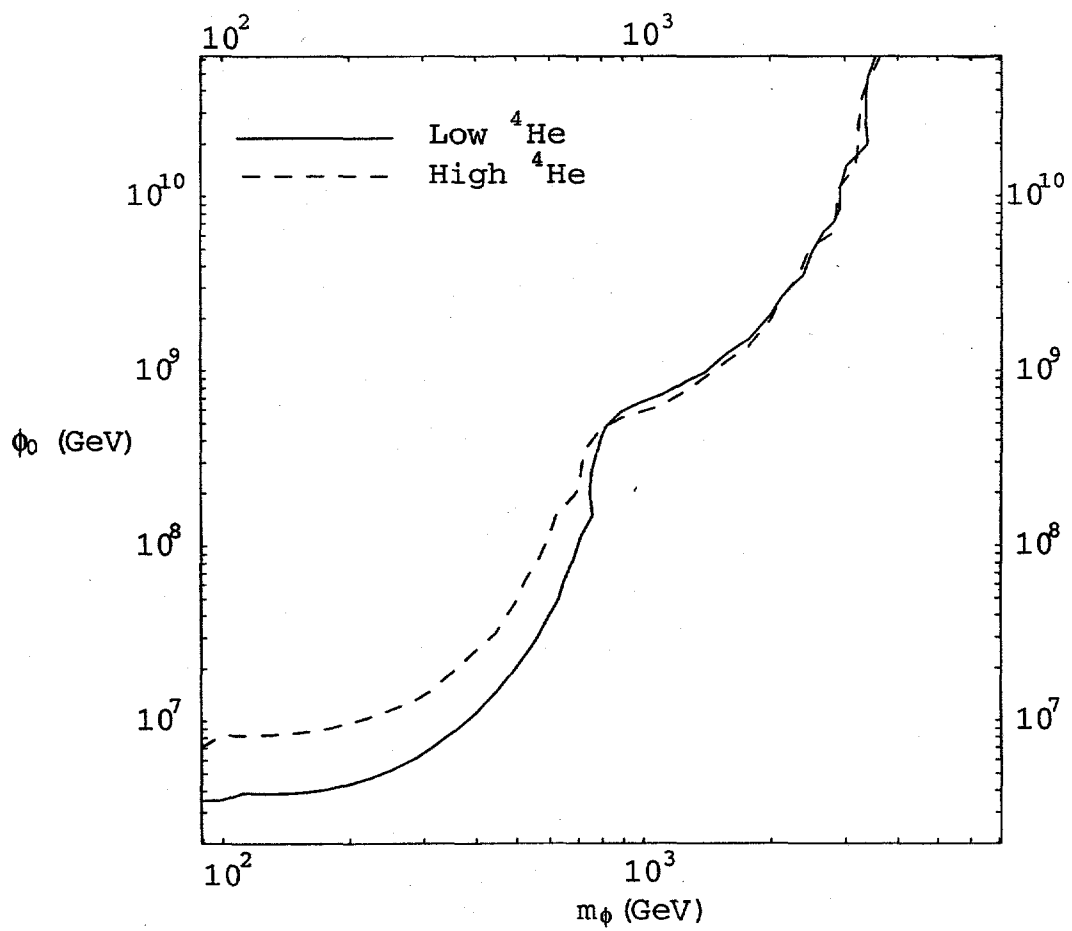
Chapter 7

Conclusion

I have discussed the photodissociation of light elements due to the radiative decay of a massive particle, and I have shown how I can constrain my model parameters from the observed light-element abundances. I adopted two quasar absorption system (QAS) D/H values, as well as solar-system data for D/H and ^{3}He/H. For each of these, I have used two ^{4}He values.

I present my results in terms of the confidence level at which each theoretical parameter set (*i.e.*, the set of properties of a radiatively decaying particle) is excluded by the observed abundances. My algorithm for computing the confidence level is consistent and general enough to apply not only to the scenarios investigated in this work, but also to many other non-standard theories of BBN.

When I adopt the low ^{4}He and low QAS D/H values, I find that a non-vanishing amount of such a long-lived, massive particle is preferred: $m_X Y_X \gtrsim 10^{-10}$ GeV for 10^4 sec $\lesssim \tau_X \lesssim 10^6$ sec. On the other hand, consistency with the observations imposes upper bounds on $m_X Y_X$ in each of the four QAS cases.

Proto-solar (D+^{3}He)/H and proto-solar ^{3}He/H prefer high η, just as low QAS D/H, so these cases (both high and low ^{4}He) resemble my analyses for low QAS D/H. However, in order to compare these observations to my theoretical calcula-

tion of the primordial light-element abundances, I need to extrapolate the observations back to the primordial abundances. To this end, I use the very general chemical evolution model of Steigman and Tosi [12]. With only a few mild assumptions, I find that for low ^{4}He, a non-vanishing abundance of long-lived, massive particles is slightly preferred. And in both the high and low ^{4}He cases, I can impose upper bounds on $m_X Y_X$.

In deriving these results, I have included the uncertainties in the light-element abundances due to the uncertainties in the nuclear reaction rates. To accomplish this, I used two algorithms: Monte-Carlo, and linear propagation of errors. Linear propagation of errors is much faster, and I have demonstrated that it yields results comparable to those of the Monte-Carlo throughout my non-standard BBN parameter space (to within a 16% difference in the error).

Another issue I have investigated is the importance of the correlations between the abundances of various elements, as the reaction rates are varied. Conventional wisdom is that these correlations may be neglected, thus simplifying the calculation. However, it has been pointed out [56] that the correlations between elements can be quite large. To resolve this question for my model, I performed my analysis with and without correlations, and compared the results. I found that correlations can safely be neglected, because they are large only in regions that are excluded by a large disagreement between theory and observation.

I have also studied the photodissociation of ^{7}Li and ^{6}Li in this dissertation. These processes do not affect the D/H and ^{4}He abundances, because ^{7}Li/H and

^{6}Li/H are many orders of magnitude less abundant than D/H and ^{4}He. When I examine the region of parameter space where the predicted abundances agree well with the observed ^{7}Li/H, the low ^{4}He, and the low QAS D/H or proto-solar (D+^{3}He)/H observations, I find that the produced ^{6}Li/H may be of order 10^{-12}, which is two orders of magnitude larger than the prediction of SBBN (see Figs. 2.5 and 4.4). The predicted ^{6}Li is consistent with the observed upper bound Eq. (3.6) throughout the region of parameter space in which I am interested. Although currently it is believed that the observed ^{6}Li is produced by spallation, my model suggests another origin: the observed ^{6}Li may be produced by the photodissociation of ^{7}Li.

Finally, I have discussed candidates for my radiatively decaying particle. My first example is the gravitino. In this case, I can constrain the reheating temperature after inflation, because it determines the abundance of the gravitino. I obtained the stringent bounds $T_R \lesssim 10^8 \text{ GeV} - 10^9 \text{ GeV}$ for $100 \text{ GeV} \lesssim m_{3/2} \lesssim 1 \text{ TeV}$. My second example is the lightest neutralino that is heavier than the gravitino. When the neutralino is the lightest superparticle in the MSSM sector, it can decay into a photon and a gravitino. If I assume the lightest neutralino is pure bino, and its mass is about 100 GeV, then the relic number density of binos is related to the right-handed slepton mass, because binos annihilate mainly through right-handed slepton exchange. For this case, I obtained an upper bound on the gravitino mass, $m_{3/2} \lesssim 700 \text{ MeV} - 4 \text{ GeV}$ for $100 \text{ GeV} \lesssim m_{\tilde{l}_R} \lesssim 1 \text{ TeV}$. My third example is a modulus field. I obtained a severe constraint on its initial amplitude:

$\phi_0 \lesssim 10^8$ GeV $- 10^9$ GeV for 100 GeV $\lesssim m_{3/2} \lesssim 1$ TeV. This bound is well below

the Planck scale, so it suggests the need for a dilution mechanism, such as thermal

inflation.

Bibliography

[1] G. Gamow, *Phys. Rev.* **70** (1946) 572; R.A. Alpher, H. Bethe, G. Gamow, *Phys. Rev.* **73** (1948) 803.

[2] D.J. Fixsen *et al.*, *Astrophys. J* **473** (1996) 576.

[3] A.G. Kim *et al.*, *Astrophys. J.* **476** (1997) L63.

[4] Particle Data Group, *The European Physical Journal* **C3** (1998) 1.

[5] T.P. Walker, G. Steigman, D.N. Schramm, K.A. Olive, and H.-S. Kang, *Astrophys. J.* **376** (1991) 51; Subir Sarkar, *Rept. Prog. Phys.* **59** (1996) 1493, hep-ph/9602260.

[6] D. Lindley, *Mon. Not. Roy. Astron. Soc.* **188** (1979) 15P; D. Lindley, *Astrophys. J.* **294** (1985) 1.

[7] H. Pagels and J.R. Primack, *Phys. Rev. Lett.* **48** (1982) 223; S. Weinberg, *Phys. Rev. Lett.* **48** (1982) 1303; L.M. Krauss, *Nucl. Phys.* **B227** (1983) 556; J. Ellis, E. Kim, and D.V. Nanopoulos, *Phys. Lett.* **B145** (1984) 181; R. Juszkiewicz, J. Silk, and A. Stebbins, *Phys. Lett.* **B158** (1985) 463; J. Ellis, E. Kim, and S. Sarkar, *Nucl. Phys.* **B259** (1985) 175; M. Kawasaki and K. Sato, *Phys. Lett.* **B189** (1987) 23; J. Ellis, G.B. Gelmini, J.L. Lopez, D.V. Nanopoulos, and S. Sarkar, *Nucl. Phys.* **B373** (1992) 399; T. Moroi, H. Murayama, and M. Yamaguchi, *Phys. Lett.* **B303** (1993) 289.

[8] M. Kawasaki and T. Moroi, *Prog. Theor. Phys.* **93** (1995) 879, hep-ph/9403364.

[9] M. Kawasaki and T. Moroi, *Astrophys. J.* **452** (1995) 506, astro-ph/9412055.

[10] S. Dimopoulos, R. Esmailzadeh, L.J. Hall, and G.D. Starkman, *Astrophys. J.* **330** (1988) 545; *Nucl. Phys.* **B311** (1989) 699.

[11] S. Dimopoulos, G. Dvali, R. Rattazzi, and G.F. Giudice, *Nucl. Phys.* **B510** (1998) 12, hep-ph/9705307.

[12] G.Steigman and M. Tosi, *Astrophys. J.* **B453** (1995) 173.

[13] S. Weinberg, *Gravitation and Cosmology: Principles and Applications of the General Theory of Relativity* (John Wiley & Sons, New York, 1972).

[14] E.W. Kolb and M.S. Turner, *The Early Universe* (Addison-Wesley, Redwood City, CA, 1990).

[15] K. Yamamoto and E. Bunn, *Astrophys. J.* **464** (1996) 8; M. White and D. Scott, *Astrophys. J.* **459** (1996) 415.

[16] S. Perlmutter *et al.*, *Astrophys. J.* **483** (1997) 565; S. Perlmutter *et al.*, *B.A.A.S.* **29** (1997) 1351, astro-ph/9812473; B.P. Schmidt *et al.*, *Astrophys. J.* **507** (1998) 46, astro-ph/9805200.

[17] G. Efstathiou *et al.*, to be published in *Mon. Not. R. Astron. Soc.* 7 May 1999, astro-ph/9812226.

[18] D.R. Tilley, H.R. Weller, and H.H. Hasan, *Nucl. Phys.* **A474** (1987) 1.

[19] F. Ajzenberg-Selove, *Nucl. Phys.* **A490** (1988) 1.

[20] F. Ajzenberg-Selove, *Nucl. Phys.* **A506** (1990) 1.

[21] F. Ajzenberg-Selove, *Nucl. Phys.* **A449** (1986) 1.

[22] M.S. Smith, L.H. Kawano, and R.A. Malaney, *Astrophys. J. Suppl. Series* **85** (1993) 219.

[23] R.V. Wagoner, *Astrophys. J. Suppl. Series* **18** (1969) 247.

[24] R.A. Malaney and W.A. Fowler, *Astrophys. J.* **345** (1989) L5.

[25] G.R. Caughlan and W.A. Fowler, *Atomic Data and Nuclear Data Tables* **40** (1988) 283.

[26] L. Kawano, *Let's Go: Early Universe II*, Fermilab preprint Pub-92/04-A (unpublished).

[27] J. Yang, M.S. Turner, G. Steigman, D.N. Schramm, and K.A. Olive, *Astrophys. J.* **281** (1984) 493.

[28] R.A. Alpher, J.W. Follin, R.C. Herman, *Phys. Rev.* **92** (1953) 1347.

[29] F. Hoyle and R.J. Tayler, *Nature* **203** (1964) 1108.

[30] P.J.E. Peebles, *Astrophys. J.* **146** (1966) 542.

[31] R.V. Wagoner, J.W. Follin, and F. Hoyle, *Astrophys. J.* **148** (1967) 3.

[32] A. Yahil and G.Beaudet, *Astrophys. J.* **206** (1976) 26; B.V. Vainer, *et al.*, *Sov. Astron.* **22** (1976) 1; Y. David and H. Reeves, in *Physical Cosmology*, eds., R. Bailin, J. Audouze, and D.N.Schramm (North-Holland, Amsterdam, 1980); N. Terasawa and K. Sato, *Astrophys. J.* **294** (1985) 9.

[33] R.V. Wagoner, *Astrophys. J.* **179** (1973) 343.

[34] D.A. Dicus, *et al.*, *Phys. Rev.* **D26** (1982) 2694.

[35] E. Holtmann, M. Kawasaki, K. Kohri, and T. Moroi, to be published in *Phys. Rev. D.*, hep-ph/9805405.

[36] N. Hata, R.J. Scherrer, G. Steigman, D. Thomas, T.P. Walker, S. Bludman, and P. Langacker, *Phys. Rev. Lett.* **75** (1995) 3977, hep-ph/9505319.

[37] K. Kohri, M. Kawasaki, and K. Sato, *Astrophys. J.* **490** (1997) 72, astro-ph/9612237.

[38] M. Kawasaki, K. Kohri, and K. Sato, *Phys. Lett.* **B430** (1998) 132, astro-ph/9705148.

[39] E. Holtmann, M. Kawasaki, and T. Moroi, *Phys. Rev. Lett.* **77** (1996) 3712, hep-ph/9603241.

[40] B.E.J. Pagel *et al.*, *Mon. Not. R. Astron. Soc.* **255** (1992) 325.

[41] K.A. Olive, G. Steigman, and E.D. Skillman, *Astrophys. J.* **483** (1997) 788.

[42] Y.I. Izotov, T.X. Thuan, and V.A. Lipovetsky, *Astrophys. J.*, **435** (1994) 647.

[43] T.X. Thuan and Y.I. Izotov, in *Primordial Nuclei and their Galactic Evolution*, edited by N. Prantzos, M. Tosi, and R. von Steiger (Kluwer Academic Publications, Dordrecht, 1998) in press.

[44] Y.I. Izotov, T.X. Thuan, and V.A. Lipovetsky, *Astrophys. J. Suppl. Series*, **108** (1997) 1.

[45] P.J. Kernan and S. Sarkar, *Phys. Rev.* **D54** (1996) R3681, astro-ph/960304.

[46] A.A. Zdziarski, *Astrophys. J.* **335** (1988) 786; R. Svensson and A.A. Zdziarski, *Astrophys. J.* **349** (1990) 415.

[47] R.D. Evans, *The Atomic Nucleus* (McGraw-Hill, New York, 1955).

[48] R. Pfeiffer, *Z. Phys.* **208** (1968) 129.

[49] D.D. Faul, B.L. Berman, P. Mayer, and D.L. Olson, *Phys. Rev. Lett.* **44** (1980) 129.

[50] A.N. Gorbunov and A.T. Varfolomeev, *Phys. Lett.* **11** (1964) 137.

[51] J.D. Irish, R.G. Johnson, B.L. Berman, B.J. Thomas, K.G. McNeill, and J.W. Jury, *Can. J. Phys.* **53** (1975) 802.

[52] C.K. Malcom, D.V. Webb, Y.M. Shin, and D.M. Skopik, *Phys. Lett.* **B47** (1973) 433.

[53] Yu.M. Arkatov, P.I. Vatset, V.I. Voloshchuk, V.A. Zolenko, I.M. Prokhorets, and V.I. Chimil', *Sov. J. Nucl. Phys.* **19** (1974) 598.

[54] B.L. Berman, *Atomic Data and Nuclear Data Tables* **15** (1975) 319.

[55] R.E. Lopez and M.S. Turner, submitted to *Phys. Rev. D*, astro-ph/9807279.

[56] P.J. Kernan and L.M. Krauss, *Phys. Rev. Lett.* **72** (1994) 3309, astro-ph/9402010.

[57] G. Fiorentini, E. Lisi, S. Sarkar, and F. L. Villante, astro-ph/9803177.

[58] A.D. Dolgov and B.E.J. Pagel, astro-ph/9711202; K. Jedamzik and G.M. Fuller, *Astrophys. J.*, **452** (1995) 33.

[59] J Lòpez-Suàrez and R. Canal, submitted to *Astrophys. J. Lett.*, astro-ph/9804235.

[60] A. Songaila, L.L. Cowie, C.J. Hogan, and M. Rugers, *Nature* **368** (1994) 599.

[61] R.F. Carswell, M. Rauch, R.J. Weymann, A.J. Cooke, and J.K. Webb, *Mon. Not. Roy. Astron. Soc.* **268** (1994) L1.

[62] M. Rugers and C.J. Hogan, *Astrophys. J., Lett.* **459** (1996) L1.

[63] M. Rugers and C.J. Hogan, *Astron. J.* **111** (1996) 2135, astro-ph/9603084; J. K. Webb *et al.*, *Nature* **388** (1997) 250; D. Tytler, S. Burles, L. Lu, X.-M. Fan, and A. Wolfe, astro-ph/9810217.

[64] R.F. Carswell, J.K. Webb, K.M. Lanzetta, *et al. Mon. Not. Roy. Astron. Soc.* **278** (1996) 506; M. Rugers and C. Hogan, *Astr. Soc. of the Pacific Conf. Series*

99 (1996) 100; E.J. Wampler, G.M. Williger, J.A. Baldwin, R.F. Carswell, C. Hazard, and R.G. McMahon *Astronomy and Astrophysics* **316** (1996) 33.

[65] G. Steigman, in *Light Element Abundances. Proceedings of an ESO/EIPC Workshop*, edited by P. Crane, (Springer, Berlin, Germany, 1995), astro-ph/9410060.

[66] D. Tytler, S. Burles, and D. Kirkman, submitted to *Astrophys. J.*, astro-ph/9612121.

[67] D. Tytler, X.-M. Fan, and S. Burles, *Nature* **381** (1996) 207, astro-ph/9603069; S. Burles and D. Tytler, submitted to *Science*, astro-ph/9603070.

[68] E.J. Wampler, *Nature* **383** (1996) 308.

[69] A. Songaila, E.J. Wampler, and L.L. Cowie, *Nature* **385** (1997) 137, astro-ph/9611143.

[70] S. Burles and D. Tytler, submitted to *Astrophys. J.*, astro-ph/9712109.

[71] F. Spite and M. Spite, *Astronomy and Astrophysics* **115** (1982), 357.

[72] P. Bonifacio and P. Molaro, *Mon. Not. Roy. Astron. Soc.* **285** (1997) 847.

[73] C.J. Hogan, astro-ph/9609138.

[74] B.D. Fields, K. Kainulainen, K.A. Olive, and D. Thomas, *New Astron.* **1** (1996) 77, astro-ph/9603009.

[75] L.M. Hobbs and J.A. Thorburn, *Astrophys. J.* **491** (1997) 772.

[76] V.V. Smith, D.L. Lambert, and P.E. Nissen, *Astrophys. J.* **408** (1993) 262.

[77] W. Hu and J. Silk, *Phys. Rev. Lett.* **70** (1993) 2661.

[78] A.P. Lightman, *Astrophys. J.* **244** (1981) 392.

[79] J. Gratsias, R.J. Scherrer, and D.N. Spergel, *Phys. Lett.* **B262** (1991) 298;
M. Kawasaki and T. Moroi, *Phys. Lett.* **B346** (1995) 27, hep-ph/9408321.

[80] D. Gautier and P. Morel, *Astronomy and Astrophysics* **B323** (1997) L9.

[81] Turck-Chièze, S. Cahen, M Cassé, and C. Doom *Astrophys. J.* **B335** (1988)
415.

[82] J. Geiss, in *Origin and Evolution of the Elements*, edited by N. Prantzos,
E. Vangioni-Flam, and M. Cassé (Cambridge University Press, Cambridge,
1993).

[83] J.L. Linsky *et al.*, *Astrophys. J.* **402** (1993) 694; P.R. McCullough, *Astrophys. J.* **390** (1992) 213.

[84] N. Hata, R.J. Scherrer, G. Steigman, D. Thomas, and T.P. Walker, *Astrophys. J.* **458** (1996) 637, hep-ph/9412087.

[85] G.Steigman and M. Tosi, *Astrophys. J.* **B401** (1992) 150.

[86] D. Bailin and A. Love, *Supersymmetric Gauge Field Theory and String Theory* (Institute of Physics Publishing, Bristol, UK, 1994).

[87] T. Moroi, *Effects of the Gravitino on the Inflationary Universe* (Ph.D. Thesis, Tohoku University, Japan, 1995), hep-ph/9503210.

[88] K.A. Olive and M. Srednicki, *Phys. Lett.* **B230** (1989) 78.

[89] B. de Carlos, J.A. Casas, F. Quevedo, and E. Roulet, *Phys. Lett.* **B318** (1993) 447, hep-ph/9308325.

[90] D.H. Lyth and E.D. Stewart, *Phys. Rev. Lett.* **75** (1995) 201, hep-ph/9502417; *Phys. Rev.* **D53** (1996) 1784, hep-ph/9510204.